


# High-energy P2-type Na-layered oxide cathode with sequentially occurred anionic redox and suppressed phase transition


Cite as: Appl. Phys. Rev. 9, 041405 (2022); <https://doi.org/10.1063/5.0100108>

Submitted: 20 May 2022 • Accepted: 17 October 2022 • Published Online: 08 November 2022

Sangyeop Lee, Jungmin Kang, Min-kyung Cho, et al.

## COLLECTIONS

 This paper was selected as Featured

 This paper was selected as Scilight



View Online



Export Citation



CrossMark

Applied  
Physics Letters

**SPECIAL TOPICS**

Submit Today!

# High-energy P2-type Na-layered oxide cathode with sequentially occurred anionic redox and suppressed phase transition



Cite as: Appl. Phys. Rev. 9, 041405 (2022); doi: 10.1063/5.0100108

Submitted: 20 May 2022 · Accepted: 17 October 2022 ·

Published Online: 8 November 2022



View Online



Export Citation



CrossMark

Sangyeop Lee,<sup>1,2</sup> Jungmin Kang,<sup>1,2</sup> Min-kyung Cho,<sup>3</sup> Hyunyoung Park,<sup>1,2</sup> Wonseok Ko,<sup>1,2</sup> Yongseok Lee,<sup>1,2</sup> Jinho Ahn,<sup>1,2</sup> Seokjin Lee,<sup>1,2</sup> Eunji Sim,<sup>4,5</sup> Kyuwook Ihm,<sup>4</sup> Jihyun Hong,<sup>6</sup> Hyungsub Kim,<sup>7</sup> and Jongsoo Kim<sup>1,2,a)</sup>

## AFFILIATIONS

<sup>1</sup>Department of Energy Science, Sungkyunkwan University, Suwon 16419, Republic of Korea

<sup>2</sup>SKKU Institute of Energy Science and Technology (SIEST), Sungkyunkwan University, Suwon 16419, Republic of Korea

<sup>3</sup>Advanced Analysis Center, Korea Institute of Science and Technology (KIST), Seoul 02792, Republic of Korea

<sup>4</sup>Nano & Interface Research Team, Pohang Accelerator Laboratory, Pohang 37673, Republic of Korea

<sup>5</sup>Department of Smart Fabrication Technology, Sungkyunkwan University, Suwon 16419, Republic of Korea

<sup>6</sup>Energy Materials Research Center, Korea Institute of Science and Technology (KIST), 14 Gil 5 Hwarang-ro, Seongbuk-gu, Seoul 02792, Republic of Korea

<sup>7</sup>Korea Atomic Energy Research Institute (KAERI), Daejeon 34057, Republic of Korea

<sup>a)</sup>Author to whom correspondence should be addressed: [jongsookim@skku.edu](mailto:jongsookim@skku.edu)

## ABSTRACT

Although anionic-redox-based layered oxide materials have attracted great attention as promising cathodes for Na-ion batteries because of their high practical capacities, they suffer from undesirable structural degradation, resulting in the poor electrochemical behavior. Moreover, the occurrence of stable anionic-redox reaction without the use of expensive elements such as Li, Co, and Ni is considered one of the most important issues for high-energy and low-cost Na-ion batteries. Herein, using first-principles calculation and various experimental techniques, we investigate the combination of vacancy ( $\square$ ) and  $Ti^{4+}$  cations in the transition-metal sites to enable outstanding anionic-redox-based electrochemical performance in the Na-ion battery system. The presence of vacancies in the P2-type  $Na_{0.56}[Ti_{0.1}Mn_{0.76}\square_{0.14}]O_2$  structure suppresses the large structural change such as the P2-OP4 phase transition, and  $Ti^{4+}$  cations in the structure result in selectively oxidized oxygen ions with structural stabilization during  $Na^+$  deintercalation in the high-voltage region. The high structural stability of P2-type  $Na_{0.56}[Ti_{0.1}Mn_{0.76}\square_{0.14}]O_2$  enables not only the high specific capacity of  $224.92 \text{ mAh g}^{-1}$  at  $13 \text{ mA g}^{-1}$  ( $1C = 264.1 \text{ mA g}^{-1}$ ) with an average potential of  $\sim 2.62 \text{ V}$  (vs  $Na^+/Na$ ) but also excellent cycle performance with a capacity retention of  $\sim 80.38\%$  after 200 cycles at  $52 \text{ mA g}^{-1}$  with high coulombic efficiencies above 99%. Although there are some issues such as low Na contents in the as-prepared state, these findings suggest potential strategies to stabilize the anionic-redox reaction and structure in layered-oxide cathodes for high-energy and low-cost Na-ion batteries.

Published under an exclusive license by AIP Publishing. <https://doi.org/10.1063/5.0100108>

## I. INTRODUCTION

With the rise of environmental pollution problems stemming from the use of fossil fuels, eco-friendly and sustainable energy generation and efficient energy storage are considered among the most important issues in the world.<sup>1–3</sup> Lithium-ion batteries (LIBs) have been widely used as energy storage systems (ESSs) for not only small electronic devices but also large-scale applications such as electric vehicles because of their high energy density and excellent power capability.<sup>4–9</sup> As this demand rapidly increases, however, the problem of

limited and concentrated Li sources is a major drawback restricting further application of LIBs to grid-scale ESSs, despite their irreplaceable merits.<sup>10</sup>

Na-ion batteries (NIBs) are considered potential alternatives to LIBs for large-scale applications because of the earth-abundant Na sources and the similar monovalent-ion-based reaction mechanism as LIBs.<sup>11–14</sup> Among the various cathode materials, such as layered oxides, polyanionic compounds, and Prussian blue analogues, P2-type Mn-based layered oxide materials (P2- $Na_xMnO_2$ ) have received great

attention as promising candidates for NIBs because of their high gravimetric capacity and the economic feasibility based on the use of the earth-abundant Mn element.<sup>15,16</sup> Moreover, it has been reported that the anionic-redox reaction of  $O^{2-}/O^-$  can occur in the  $P2-Na_xMnO_2$  structure during  $Na^+$  de/intercalation through the substitution of Mn cations for redox-inactive metals such as Mg, Zn, and Li.<sup>17–19</sup> However, unlike Li-rich layered oxide cathodes based on reversible de/intercalation of above 1 mol  $Li^+$ , the theoretically available  $Na^+$  content in  $P2-Na_xMnO_2$  is only 1 mol regardless of the occurrence of the anionic redox reaction, which is similar to those in other layered oxide cathode materials based on the cationic redox reaction of transition-metal (TM) ions. The use of Li as the redox-inactive metal for the anionic redox reaction can result in an increase in the theoretical gravimetric capacity of  $P2-Na_xMnO_2$  by decreasing the molar mass upon substitution of the heavy element Mn with the very light element Li. However, the application of Li for the anionic-redox reaction is accompanied by an increase in the production cost of NIBs.

Recently, it was reported that the  $O^{2-}/O^-$  redox reaction can occur in the high-voltage region through the formation of vacancies ( $\square$ ) in the TM layers of the  $Na_xMnO_2$  structure.<sup>20–22</sup> Simply lowering the Mn content by introducing vacancies can result in an increase in the theoretical gravimetric capacity and energy density of the anionic-redox-based  $P2-Na_xMnO_2$  cathode. Furthermore, it was reported that the phase transition from P2 to OP4 phase could be occurred since the prismatic sites become thermodynamically unstable after most of  $Na^+$  are deintercalated from the crystal structure of P2-type layered oxides.<sup>23</sup> Since the anionic redox reaction in P2-type layered oxide is occurred at the high state of charge after oxidation to  $Mn^{4+}$  and the corresponding  $Na^+$  deintercalation, the common anionic-redox-based P2-type layered oxide cathodes experience P2-OP4 phase transition during charging to high voltage region.<sup>24–26</sup> With occurrence of P2-OP4 phase transition, the existing P2 (002) peak was disappeared, and the new OP4 (004) peak was observed at the high  $2\theta$  value. However, it was reported that the existence of vacancies in the TM site can provide the buffer to suppress the local structural distortion by formation of oxidized oxygen anions during charge/discharge.<sup>27,28</sup> Thus, the P2-type layered oxide with vacancies in the TM site does not undergo large structural change such as P2-OP4 phase transition,<sup>22,29,30</sup> which is considered one of the important merits of vacancy-containing material, enabling more stable cycle performance during prolonged cycling. However, the anionic redox reaction accompanies the undesirable structural deformation through the formation of oxidized oxygen anions and the sluggish kinetics during charge/discharge, resulting in poor electrochemical behaviors of the cathode materials with high theoretical capacities.<sup>31,32</sup> Thus, enhancement of the structural stability of anionic-redox-based cathode materials is necessary to achieve outstanding cycle performance and power capability with large practical capacity and energy density.

In this study, we demonstrated that the combination of vacancies and  $Ti^{4+}$  cations in the (TM) layers of  $P2-Na_x[Mn_{1-y}\square_y]O_2$  enables not only a large available capacity based on the remarkably stable  $O^{2-}/O^-$  redox reaction but also excellent electrochemical properties via high structural stability. Through combined first-principles calculation and various experiment techniques, including *ex situ/operando* x-ray diffraction (XRD), x-ray absorption near edge structure (XANES) spectroscopy, extended x-ray absorption fine structure (EXAFS) spectroscopy, and soft x-ray absorption spectroscopy (sXAS), it was

revealed that  $Ti^{4+}$  cations with fixed oxidation state during charge/discharge can play a critical role as a structural stabilizer, resulting in selectively oxidized oxygen anions and stable electrochemical behavior. At a current density of  $13\text{ mA g}^{-1}$  ( $1C = 264.1\text{ mA g}^{-1}$ ),  $P2-Na_{0.56}[Ti_{0.1}Mn_{0.76}\square_{0.14}]O_2$  (P2-NTMVO) delivered a large specific capacity of  $\sim 224.92\text{ mAh g}^{-1}$  with an average voltage of  $\sim 2.62\text{ V}$  (vs  $Na^+/Na$ ), which is larger than that of other cathode materials for NIBs. In particular, after 200 cycles, up to  $\sim 80.38\%$  of the initial capacity of P2-NTMVO was retained with a highly stable  $O^{2-}/O^-$  redox reaction and suppressed voltage decay, which is more outstanding than the cycle performance of  $P2-Na_{0.56}[Mn_{0.86}\square_{0.14}]O_2$  (P2-NMVO) with poor capacity retention of  $\sim 60.44\%$  under the same conditions. Even at  $650\text{ mA g}^{-1}$ , P2-NTMVO delivered a specific capacity of  $\sim 137.3\text{ mAh g}^{-1}$ , corresponding to  $\sim 61\%$  of the capacity measured at  $13\text{ mA g}^{-1}$ , indicating the outstanding power capability of P2-NTMVO. Furthermore, the economic feasibility of the composition based on earth-abundant Na, Mn, and Ti is one of the attractive advantages of P2-NTMVO as a promising cathode for low-cost and high-energy NIBs.

## II. EXPERIMENTAL SECTION

### A. Preparation of material

The  $P2-Na_{0.56}[Ti_xMn_{0.86-x}\square_{0.14}]O_2$  ( $x = 0$  or  $0.1$ ) compounds were synthesized through the conventional solid-state method.  $NaNO_3$  (Alfa Aesar, 99%),  $TiO_2$  (Sigma Aldrich, 99%), and  $MnCO_3$  (Alfa Aesar, 98%) precursors were used. The molar ratios of the precursors used for the preparation of  $P2-Na_{0.56}[Ti_xMn_{0.86-x}\square_{0.14}]O_2$  ( $x = 0$  or  $0.1$ ) are as follows:  $Na:Ti:Mn = 0.588 (= 0.56 \times 1.05):x:0.86-x$  ( $x = 0$  or  $0.1$ ), which indicate the usage of 5%-excess Na-based precursors compared to the stoichiometric amounts. It was reported that adding  $\sim 5\%$  excess of Na precursor was required to compensate for the loss of Na during the calcination process at high temperature.<sup>33–36</sup> As a result of inductively coupled plasma (ICP) measurement (Table S1), it was confirmed that  $P2-Na_{0.56}[Ti_xMn_{0.86-x}\square_{0.14}]O_2$  was successfully synthesized with the 0.56 mol Na contents through adding the additional  $\sim 5\%$  Na precursor. The total weigh of 10 g of the precursors, 100 ml of ethanol (Samchun, 99%), and 15 zirconia ball ( $\varnothing 10\text{ mm}$ ) was sealed in a nalgene low density polyethylene (LDPE) bottle, and they were mixed uniformly using ball-milling machine (Wisd, BML-2) at 250 rpm for 12 h. After mixing, the obtained mixture was dried at  $120^\circ\text{C}$  in the forced conventional oven (JEIO TECH, OF-11E) for 12 h. The dried mixture was pelletized under 300 bar and calcined at  $630^\circ\text{C}$  ( $5^\circ\text{C}/\text{min}$  of heating rates) for 12 h under  $0.31\text{ min}^{-1}$  flow of  $O_2$  gas and then slowly cooled down to  $200^\circ\text{C}$  ( $1^\circ\text{C}/\text{min}$  of cooling rates) in the same  $O_2$  condition. After cooling, the powder was immediately moved to the Ar-filled glovebox to avoid the moisture contact in the air condition.

### B. Materials characterization

The  $P2-Na_{0.56}[Ti_xMn_{0.86-x}\square_{0.14}]O_2$  ( $x = 0$  or  $0.1$ ) structures and *operando* XRD patterns were analyzed using XRD (PANalytical, EMPYREAN) with  $Mo\ K\alpha$  radiation ( $\lambda = 0.70932\text{ \AA}$ ). The  $2\theta$  range was  $4.61^\circ\text{--}34.32^\circ$  with a step size of  $0.01^\circ$ , and the patterns were converted angles with  $Cu\ K\alpha$  radiation ( $\lambda = 1.54178\text{ \AA}$ ). Rietveld refinement<sup>37</sup> was performed using the FullProf software based on the XRD data. The *operando* XRD patterns of  $P2-Na_{0.56}[Ti_xMn_{0.86-x}\square_{0.14}]O_2$  ( $x = 0$  or  $0.1$ ) were obtained during electrochemical testing at a current

density of  $30 \text{ mA g}^{-1}$  within the voltage range of 4.5–1.5 V (vs  $\text{Na}^+/\text{Na}$ ). Neutron diffraction (ND) was conducted from the HANARO facility at the Korea Atomic Energy Research Institute (KAERI). The  $2\theta$  range was  $0^\circ$ – $160^\circ$  with a step size of  $0.05^\circ$ , and the neutron wavelength was  $1.83458 \text{ \AA}$ . The atomic ratios of elements such as Na, Ti, and Mn were confirmed using an inductively coupled plasma-atomic emission spectrometer (ICP-AES) at the National Center for Inter-university Research Facilities (NCIRF) at Seoul National University. The presence of vacancies in  $\text{P2-Na}_{0.56}[\text{Ti}_x\text{Mn}_{0.86-x}\square_{0.14}]\text{O}_2$  ( $x = 0$  or  $0.1$ ) was confirmed using scanning transmission electron microscopy-high-angle annular dark field (STEM-HAADF) analysis at the Korea Institute of Science and Technology (KIST). In addition, the particle size, morphology, and weight ratio of each element were identified using SEM (JSM-7800F Prime). Transmission electron microscopy-energy-dispersive x-ray spectroscopy (TEM-EDS) analysis was conducted at NCIRF. The valence states of Mn and Ti in the structure of  $\text{P2-Na}_{0.56}[\text{Ti}_x\text{Mn}_{0.86-x}\square_{0.14}]\text{O}_2$  ( $x = 0$  or  $0.1$ ) during charge/discharge were determined from XANES analysis performed at beamline 6D and 8C at the Pohang Accelerator Laboratory (PAL), South Korea, with an electron energy of 2.5 GeV and 200 mA of current. To verify the oxidation state of transition metal (TM) ions through XAENS spectra, we compare the energy level of the K-edge in XANES spectra among the target samples and the reference materials.<sup>38,39</sup> To confirm the valence state of O, *ex situ* sXAS spectra were obtained by 4D at PAL with 525–560 eV photon range. The collected data of XANES and sXAS were analyzed using the Athena software. Additionally, x-ray photoelectron spectroscopy (XPS) was performed at SKKU to confirm the Mn, Ti valence states and oxygen redox reaction.

### C. Electrochemical characterization

The electrodes of  $\text{P2-Na}_{0.56}[\text{Ti}_x\text{Mn}_{0.86-x}\square_{0.14}]\text{O}_2$  ( $x = 0$  or  $0.1$ ) were prepared by mixing 70 wt. % active material, 10 wt. % carbon nanotube (CNT) dispersion, 10 wt. % Super P carbon black, and 10 wt. % polyvinylidene fluoride (PVDF) using N-methyl-2-pyrrolidone (NMP) as the solvent. Since it was known anionic redox reaction of  $\text{O}^{2-}/\text{O}^-$  deliver poorer kinetics than normal cationic redox reaction of transition metal (TM) ions,<sup>31,32</sup> we applied 20 wt. % of conductive carbons for the fabrication of the electrode. The mixed slurry was applied evenly on Al foil using a doctor blade, and the electrodes were dried at  $100^\circ\text{C}$  for 24 h in a vacuum oven. The loading mass of the electrode was  $\sim 2 \text{ mg cm}^{-2}$ . CR2032 cells were fabricated using a  $\text{P2-Na}_{0.56}[\text{Ti}_x\text{Mn}_{0.86-x}\square_{0.14}]\text{O}_2$  ( $x = 0$  or  $0.1$ ) electrode, a separator (Whatman GF/F glass fiber), Na metal as the counter electrode, and 1.0 M  $\text{NaPF}_6$  in propylene carbonate (PC):fluoroethylene carbonate (FEC) in a volume ratio of 98:2 as the electrolyte in an Ar-filled glovebox. Galvanostatic electrochemical tests were performed at various C-rates (13–650  $\text{mA g}^{-1}$ ) in the voltage range of 1.5–4.5 V (vs  $\text{Na}^+/\text{Na}$ ) using an automatic charge/discharge system (WBCS 3000, WonATech). The energy density ( $\text{Wh kg}^{-1}$ ) was calculated by integral of the discharge profile based on capacity ( $\text{mAh g}^{-1}$ ) and voltage (V). The cycle performance was measured at  $52 \text{ mA g}^{-1}$  in the voltage range of 1.5–4.5 V (vs  $\text{Na}^+/\text{Na}$ ) after the first charge/discharge at  $13 \text{ mA g}^{-1}$ . It was measured at a low current, so that the anion reduction reaction sufficiently occurred, and the cycle performance was additionally measured at a high current density condition of  $650 \text{ mA g}^{-1}$ .

### D. Computational details

All the density functional theory (DFT) calculations of  $\text{P2-Na}_{0.56}[\text{Ti}_{0.1}\text{Mn}_{0.76}\square_{0.14}]\text{O}_2$  were performed using the Vienna *Ab initio* Simulation Package (VASP).<sup>40</sup> The projector-augmented wave (PAW) pseudopotentials were used through the plane wave basis embedded in the VASP.<sup>41</sup> The exchange–correlation functional was expressed using the generalized gradient approximation (GGA) of the Perdew–Burke–Ernzerhof (PBE) parameterization. For the DFT calculations, a  $3 \times 3 \times 1$  supercell structure of  $\text{P2-Na}_{0.56}[\text{Ti}_{0.1}\text{Mn}_{0.76}\square_{0.14}]\text{O}_2$  was calculated using a  $4 \times 4 \times 3$  k-point grid. GGA+U<sup>42,43</sup> was adopted to represent the localization of the d-orbital in Ti, Mn ions with  $U_{\text{eff}}$  of 1.5 and 3.9 eV, respectively.

CASM<sup>44</sup> software was used to generate all the  $\text{Na}^+$  configurations at each composition, and the full density functional theory (DFT) calculations were conducted for a maximum of 20 configurations. The convex-hull plot of  $\text{P2-Na}_{0.56}[\text{Ti}_{0.1}\text{Mn}_{0.76}\square_{0.14}]\text{O}_2$  was obtained with the lowest energy for each composition.

## III. RESULTS AND DISCUSSION

### A. Structural information for P2-NTMVO with vacancy in (TM) layers

To prepare vacancies in the transition metal (TM) site in the P2-type layered structure, it should be required to get the high oxidation state of TM cations such as  $\text{Mn}^{4+}$  and  $\text{Ti}^{4+}$  during the synthesis process, due to the charge neutrality of  $\text{P2-Na}_y[\text{TM}_{1-x}\square_x]\text{O}_2$  composition. Moreover, the Na contents in  $\text{P2-Na}_y[\text{TM}_{1-x}\square_x]\text{O}_2$  are also determined by the vacancy contents, and the Na contents should be decreased with increase in the vacancy contents for the charge neutrality. To prepare the P2 phase, in particular, Na-deficiency in the structure ( $0.3 \leq \text{Na} \leq 0.7$ ) is also required.<sup>23</sup> Thus, to get adequate Na and vacancy contents in the P2 phase simultaneously, we designed  $\text{P2-Na}_{0.56}[\text{Ti}_{0.1}\text{Mn}_{0.76}\square_{0.14}]\text{O}_2$  with 0.14 mol vacancies. The detailed structural information  $\text{P2-Na}_{0.56}[\text{Ti}_{0.1}\text{Mn}_{0.76}\square_{0.14}]\text{O}_2$  (P2-NTMVO) was confirmed through Rietveld refinement based on the x-ray diffraction (XRD) pattern [Fig. 1(a)]. P2-NTMVO was characterized as a P2-type layered structure with  $\text{P6}_3/\text{mmc}$  space group, and any impurities or second phases were not detected. The lattice parameters of P2-NTMVO were calculated to be  $a = b = 2.87333(8) \text{ \AA}$  and  $c = 11.1289(7) \text{ \AA}$  with low values of reliability factors ( $R_p = 3.38\%$ ,  $R_1 = 2.16\%$ ,  $R_f = 3.91\%$ , and  $\chi^2 = 3.85\%$ ). To quantify the amount of vacancy in  $\text{P2-Na}_{0.56}[\text{Ti}_{0.1}\text{Mn}_{0.76}\square_{0.14}]\text{O}_2$  more accurately, we performed neutron diffraction (ND) analyses (Fig. S1). Detailed structural information for the P2-NTMVO compounds such as the atomic positions, occupancies, and  $B_{\text{iso}}$  factor is provided in Table S2, and it was verified that the occupancies of Mn and Ti elements in the transition metal (TM) site are 0.760(7) and 0.099(5), respectively, which means there are  $\sim 0.14$  mol vacancies in the TM site of  $\text{P2-Na}_{0.56}[\text{Ti}_{0.1}\text{Mn}_{0.76}\square_{0.14}]\text{O}_2$ . In addition, the Na occupancy was negligible at the TM sites, indicating that Na could not enter the TM sites, which is attributed to the larger ionic radius of  $\text{Na}^+$  ( $\sim 1.02 \text{ \AA}$ ) than those of TM ions such as  $\text{Mn}^{4+}$  ( $\sim 0.53 \text{ \AA}$ ) and  $\text{Ti}^{4+}$  ( $\sim 0.605 \text{ \AA}$ ).<sup>45</sup> In addition, through selected-area electron diffraction (SAED) analyses [Fig. 1(b)], it was confirmed that P2-NTMVO was well prepared with single-crystalline particles with a P2-type layered structure showing the (002) and (100) planes along the  $[0\bar{1}0]$  direction.

To confirm the presence of vacancies in the P2-NTMVO structure, we performed scanning transmission electron microscopy-high-angle



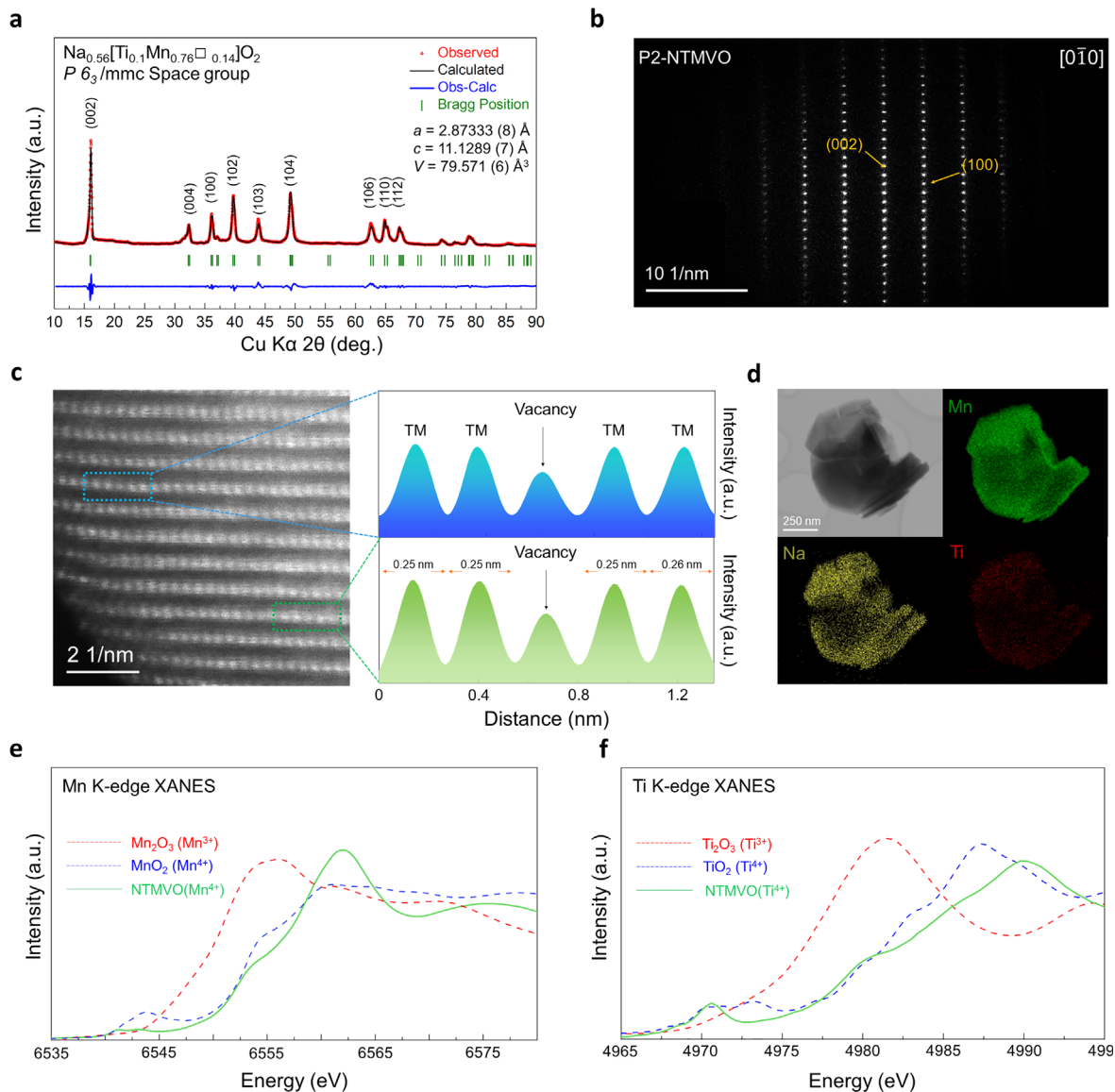


**FIG. 1.** (a) Refined XRD patterns of P2- $\text{Na}_{0.56}[\text{Ti}_{0.1}\text{Mn}_{0.76}\square_{0.14}]\text{O}_2$ . (b) SAED patterns of P2- $\text{Na}_{0.56}[\text{Ti}_{0.1}\text{Mn}_{0.76}\square_{0.14}]\text{O}_2$ . (c) STEM-HAADF image of P2- $\text{Na}_{0.56}[\text{Ti}_{0.1}\text{Mn}_{0.76}\square_{0.14}]\text{O}_2$  and signal profile of enclosed regions by the dotted line. (d) TEM-EDS map of P2- $\text{Na}_{0.56}[\text{Ti}_{0.1}\text{Mn}_{0.76}\square_{0.14}]\text{O}_2$ . *Ex situ* XANES spectra of P2- $\text{Na}_{0.56}[\text{Ti}_{0.1}\text{Mn}_{0.76}\square_{0.14}]\text{O}_2$  at the (e) Mn K-edge and (f) Ti K-edge.

annular dark field (STEM-HAADF) analysis. In the STEM-HAADF image [Fig. 1(c)], signals with relatively weak intensity appeared irregularly in the (TM) layers. In terms of Ti cations, their signals in the electron-microscopy-based analyses were similar to the signals of the Mn cations because of their similar atomic number. Thus, these STEM-HAADF results indicate that the vacancies are randomly arranged in the (TM) layers of the P2-NTMVO structure.<sup>46,47</sup> Moreover, transmission electron microscopy (TEM) and energy-dispersive x-ray spectroscopy (EDS) elemental mapping analyses [Fig. 1(d)] revealed that Na, Mn, and Ti elements were homogeneously distributed in the P2-NTMVO particles with a size of  $\sim 500$  nm, and the

atomic ratio of Na, Ti, and Mn in the P2-NTMVO particles was  $\sim 0.560:0.098:0.761$ . This atomic ratio and particle size of P2-NTMVO were consistent with the inductively coupled plasma atomic emission spectroscopy (ICP-AES) and scanning electron microscopy (SEM) results, respectively [Table S1(a) and Fig. S2]. To prepare the vacancy-contained P2- $\text{Na}_{0.56}[\text{Ti}_{0.1}\text{Mn}_{0.76}\square_{0.14}]\text{O}_2$ , it is essential to control the gas condition during calcination. Through the energy dispersive x-ray spectroscopy based on scanning electron microscopy (SEM-EDS) analyses (Fig. S3 and Table S3), it was verified that the atomic ratio of (Mn + Ti): O after calcination in  $\text{O}_2$  gas condition is  $\sim 0.86:2$ , which is different from that after calcination in the air condition ( $\sim 0.90:2$ ).

This result on the atomic ratio of Mn: O in P2-Na<sub>0.56</sub>[Ti<sub>0.1</sub>Mn<sub>0.76□0.14</sub>]O<sub>2</sub> is also consistent with the results of ND- and XRD-based Rietveld refinement. Since lowering atomic ratio of Mn:O indicates increased vacancy contents in the TM site, we confirmed that the calcination process under O<sub>2</sub> gas condition should be required for preparation of P2-Na<sub>0.56</sub>[Ti<sub>0.1</sub>Mn<sub>0.76□0.14</sub>]O<sub>2</sub>. Moreover, we arranged the simulated intensity ratios between (100) and (103) XRD peaks depending on the vacancy contents in the Mn site and then compared them with the real intensity ratio of the samples prepared under the O<sub>2</sub> gas and the air condition. As shown in Fig. S4, it was revealed that the sample based on the O<sub>2</sub> gas has ~0.14 mol vacancies in the Mn site, whereas the sample based on the air condition just delivers ~0.12 mol vacancies. Furthermore, Rietveld refinement results on the XRD pattern of the sample prepared under the air condition indicate that there are just ~0.12 mol vacancies in the Mn site (Fig. S5 and Table S4).

In the x-ray absorption near edge structure (XANES) results [Figs. 1(e) and 1(f)], it was verified that each Mn K-edge and Ti K-edge XANES spectra of P2-NTMVO have similar energy levels with those of Mn<sup>(4+)</sup>O<sub>2</sub> and Ti<sup>(4+)</sup>O<sub>2</sub> rather than Mn<sup>(3+)</sup><sub>2</sub>O<sub>3</sub> and Ti<sup>(3+)</sup><sub>2</sub>O<sub>3</sub>, which indicates that both oxidation states of Mn and Ti ions in P2-NTMVO are close to +4. Moreover, we performed x-ray photoelectron spectroscopy (XPS) analysis to confirm the valence state of transition metal. Figure S6 shows that the binding energies of Mn and Ti ions in P2-Na<sub>0.56</sub>[Ti<sub>0.1</sub>Mn<sub>0.76□0.14</sub>]O<sub>2</sub> are ~642.5 and ~458.8 eV, respectively, which is consistent with those of Mn<sup>4+</sup>- and Ti<sup>4+</sup>-based materials.<sup>48,49</sup> These results are also considered as further evidence supporting the existence of vacancies in (TM) layers of P2-NTMVO because of the requirement of Mn<sup>4+</sup> and Ti<sup>4+</sup> cations in P2-NTMVO for the charge neutrality of the Na<sup>[+]</sup><sub>0.56</sub>[Ti<sup>[4+]</sup><sub>0.1</sub>Mn<sup>[4+]</sup><sub>0.76□0.14</sub>]O<sup>[2-]</sup><sub>2</sub> composition. Additionally, we confirm the valence state of Mn (+4) and performed a chemical titration experiment (Table S5).<sup>50–52</sup> As a result of the oxalic acid-permanganate back titration, the average of the coefficient values *x* was 2.00 ± 0.01, which means that the average valence state of Mn in P2-NTMVO is tetravalent (+4).

In addition, we prepared P2-Na<sub>0.56</sub>[Mn<sub>0.86□0.14</sub>]O<sub>2</sub> (P2-NMVO) to confirm the effect of Ti<sup>4+</sup> cations as the structural stabilizer in the P2-NTMVO structure. The XRD, SAED, and SEM measurements indicate that P2-NMVO exhibits a similar P2-type layered structure and morphology as P2-NTMVO (Figs. S7–S9). Moreover, through the refined structural information and STEM-HAADF analyses (Table S6 and Fig. S10), it was verified that vacancies exist in the (TM) layers of the P2-NMVO structure. The low values of reliability factors on Rietveld refinement of P2-NMVO (*R*<sub>p</sub> = 3.76%, *R*<sub>i</sub> = 4.58%, *R*<sub>f</sub> = 4.77%, and  $\chi^2$  = 2.33%) indicate the high accuracy of the Rietveld refinement. ICP-AES and TEM-EDS mapping analyses also show the homogenous Na and Mn distribution in ~700 nm sized P2-NMVO particles with an elemental ratio of Na:Mn = ~0.560:0.859 [Table S1(b) and Fig. S11].

## B. Excellent electrochemical properties of P2-NTMVO

Figures 2(a) and 2(b) show the electrochemical performances of P2-NTMVO and P2-NMVO at various current densities in the voltage range of 1.5–4.5 V (vs Na<sup>+</sup>/Na). The initial discharge capacities of P2-NTMVO and P2-NMVO at 13 mA g<sup>-1</sup> (1C = 264.1 and 262.2 mA g<sup>-1</sup>) were ~224.92 and ~219 mAh g<sup>-1</sup>, respectively, which indicates the larger available Na<sup>+</sup> content of P2-NTMVO relative to

that of P2-NMVO during charge/discharge. Even at the high current density of 650 mA g<sup>-1</sup>, P2-NTMVO maintained a specific capacity of up to ~137.3 mA g<sup>-1</sup>, whereas that of P2-NMVO was only ~107.6 mA g<sup>-1</sup> under the same conditions. These results imply that the presence of Ti<sup>4+</sup> cations in vacancy-contained P2-type Mn-based layered oxides enables better power capability. In addition, we attempted to measure the electrochemical performances of P2-NTMVO under the full cell system. It was known that the Na-deficient cathode materials can deliver the half-cell-based large capacity under the full-cell system through the following methods: (1) application of sodiated anode materials and (2) usage of sacrificing sodium additives.<sup>53,54</sup> Thus, to investigate the possibility on the application of P2-NTMVO as the cathode in the realistic full cell system, we performed the full-cell test using the sodiated hard carbon anode. As shown in Fig. S12, it was verified that the P2-NTMVO-based full cell exhibited the large specific capacity of ~169.8 mAh g<sup>-1</sup> at 52 mA g<sup>-1</sup> in the voltage range of 1.4–4.4 V (vs Na<sup>+</sup>/Na), which is highly similar with the half-cell-based capacity. Moreover, the capacity under the full cell system was maintained up to ~91.2% of the initial capacity after 100 cycles, which indicates the outstanding electrochemical performances of P2-NTMVO cathode in the realistic full cell system. Moreover, the merit of Ti<sup>4+</sup> cations in terms of enhancing the electrochemical behaviors stands out upon comparison of the cycle performances of P2-NTMVO and P2-NMVO. As shown in Figs. 2(c) and S13, up to ~80.38% of the initial specific capacity of P2-NTMVO was maintained with a high coulombic efficiency of above 99% after 200 cycles at 52 mA g<sup>-1</sup>, which is clearly distinguished from the poor cycle performance of P2-NMVO, which only exhibited a capacity retention of ~60.44% under the same conditions. Moreover, as a result of cycle performance at a high current density of 650 mA g<sup>-1</sup>, the Ti-containing sample showed 86.7% capacity retention compared to the initial capacity with 99% coulombic efficiency, and P2-NMVO showed 64.3% capacity retention (Fig. S14). To demonstrate the role of the vacancy in the structure, furthermore, we prepared P2-Na<sub>0.56</sub>[Mn<sub>0.89□0.11</sub>]O<sub>2</sub> [P2-NMVO\_11 (□: 0.11 mol)] having the different amounts of vacancies compared to existing P2-NMVO having the 0.14 mol vacancies. Through Rietveld refinement and XRD analyses, we confirmed that P2-NMVO\_11 exhibits the phase-pure P2-type layered structure with no impurities, and there are ~0.11 mol vacancies in the Mn site (Fig. S15 and Table S7). Furthermore, the result of Rietveld refinement of P2-NMVO\_11 was calculated with low reliability factors (*R*<sub>p</sub> = 2.87%, *R*<sub>i</sub> = 4.37%, *R*<sub>f</sub> = 4.84%, and  $\chi^2$  = 4.27%), indicating high accuracy. In addition, the difference of vacancy contents in the Mn site affects the intensity ratio of some XRD peaks. Through comparison of the intensity ratios between (100) and (103) XRD peaks (Fig. S16), it was clearly verified that there are ~0.11 and ~0.14 mol vacancies in the Mn site of P2-NMVO\_11 and P2-NMVO, respectively. In terms of electrochemical performances of P2-NMVO\_11, the specific capacity was retained to just ~64.3% of the initial capacity after 100 cycles at 52 mA g<sup>-1</sup> (Fig. S17), which indicates poorer cycle performance of P2-NMVO\_11 than not only P2-Na<sub>0.56</sub>[Ti<sub>0.1</sub>Mn<sub>0.76□0.14</sub>]O<sub>2</sub> (P2-NTMVO) but also P2-NMVO. Moreover, Fig. S18 shows the initial charge/discharge capacities of P2-NMVO\_11, which are also lower than those of P2-NMVO. Na de/intercalation from P2-NMVO\_11 and P2-NMVO is mainly affected by anionic redox reaction of O<sup>2-</sup>/O<sup>-</sup>. Thus, it is important to stabilize anionic redox reaction of O<sup>2-</sup>/O<sup>-</sup> to improve

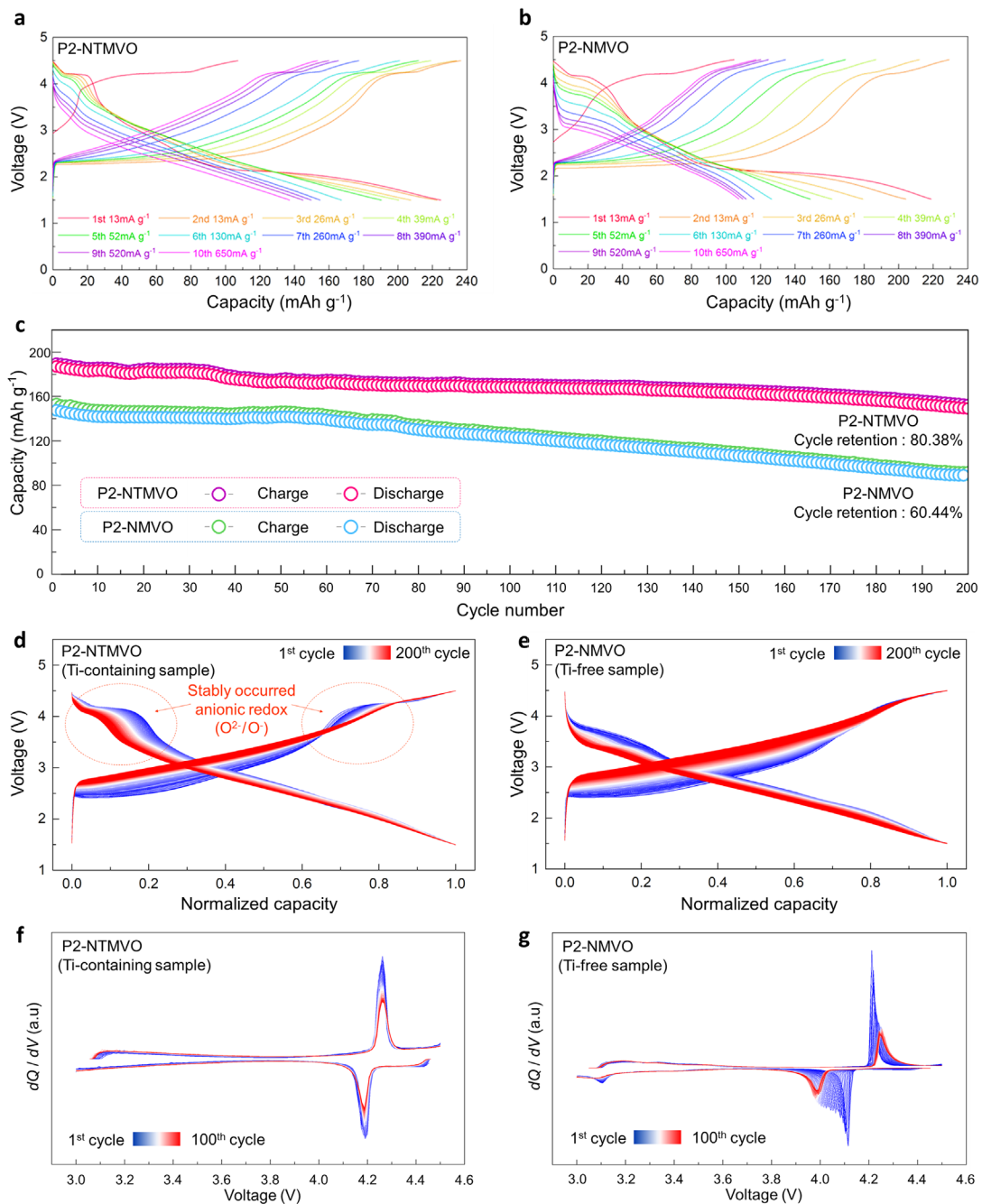


**FIG. 2.** Charge/discharge curves of (a) P2-Na<sub>0.56</sub>[Ti<sub>0.1</sub>Mn<sub>0.76</sub>□<sub>0.14</sub>]O<sub>2</sub> and (b) P2-Na<sub>0.56</sub>[Mn<sub>0.86</sub>□<sub>0.14</sub>]O<sub>2</sub> in the voltage range of 1.5–4.5 V at various discharge current rates. (c) Comparison of cycling performance of P2-Na<sub>0.56</sub>[Ti<sub>0.1</sub>Mn<sub>0.76</sub>□<sub>0.14</sub>]O<sub>2</sub> and P2-Na<sub>0.56</sub>[Mn<sub>0.86</sub>□<sub>0.14</sub>]O<sub>2</sub> over 200 cycles at 52 mA g<sup>-1</sup>. Comparison of normalized capacity profile for 200 cycles in (d) Ti-containing sample and (e) Ti-free sample. dQ/dV profile of (f) P2-Na<sub>0.56</sub>[Ti<sub>0.1</sub>Mn<sub>0.76</sub>□<sub>0.14</sub>]O<sub>2</sub> and (g) P2-Na<sub>0.56</sub>[Mn<sub>0.86</sub>□<sub>0.14</sub>]O<sub>2</sub> during 100 cycles.

the available capacities and cyclability of P2-NMVO. It was reported that vacancies in the TM site can play a role as the buffer to suppress the local structural distortion attributed to oxidized oxygen anions formed during anionic redox reaction.<sup>27,28</sup> Thus, since increased contents of vacancies in the TM site can result in

more stable anionic redox reaction of O<sup>2-</sup>/O<sup>-</sup>, P2-NMVO can deliver higher capacity and better capacity retention than P2-NMVO<sub>11</sub>. These results indicate that vacancies in the P2-NMVO structure can play an important role for improving the reversibility of anion redox.

In particular, comparison of the normalized charge/discharge profiles between P2-NTMVO and P2-NMVO [Figs. 2(d) and 2(e)], it clearly reveals the more stable anionic redox reaction of  $O^{2-}/O^-$  in P2-NTMVO with  $Ti^{4+}$  cations as a structural stabilizer relative to that in P2-NMVO. For prolonged cycling, the hysteresis between charge and discharge near 4.2 V indicating  $O^{2-}/O^-$  redox reaction increased in the Ti-free sample, whereas the profile was stably retained in the Ti-containing sample. Thus, it was confirmed that P2-NTMVO can deliver better electrochemical behavior with stabilized anionic redox reaction than P2-NMVO through the presence of the structural stabilizer, Ti cations in vacancy-contained P2-type Mn-based layered oxides. Moreover, the overall crystal structure of P2-NTMVO (Fig. S19) was well maintained after 200 cycles with the anionic-redox reaction occurring in the high-voltage region, which also implies the high structural stability of P2-NTMVO enabling the stabilized anionic redox reaction. On the other hand, the XRD pattern of P2- $Na_{0.56}[Mn_{0.86}\square_{0.14}]O_2$  was highly degraded after 100 cycles (Fig. S20), which indicates that large structural change was occurred in P2- $Na_{0.56}[Mn_{0.86}\square_{0.14}]O_2$  structure after 100 cycles. In 100-cycled XRD pattern of P2- $Na_{0.56}[Mn_{0.86}\square_{0.14}]O_2$ , however, we cannot detect formation of new phases different from P2 phase, implying the TM migration to Na layer, which could be attributed to the instability of TM ions in prismatic sites of Na ions and the larger ionic radius of  $Na^+$  than those of TM ions.<sup>55,56</sup> Through the STEM-HAADF analyses, it was verified that the 100-cycled P2- $Na_{0.56}[Mn_{0.86}\square_{0.14}]O_2$  sample was overall composed of P2 phase without severe TM migration to Na layers (Fig. S21). These results imply that the cycle performance of P2- $Na_{0.56}[Mn_{0.86}\square_{0.14}]O_2$  was not highly affected by TM migration to the Na layer. TM migration to the Na layer cannot severely affect the

cycle performance of P2- $Na_{0.56}[Mn_{0.86}\square_{0.14}]O_2$ . In addition, we performed the cycle test at the high voltage region of 3.0–4.5 V (vs  $Na^+/Na$ ) related to anion redox of  $O^{2-}/O^-$ . As shown in Fig. S22, P2-NTMVO exhibited the capacity retention of  $\sim 99.16\%$  compared to the initial capacity after 100 cycles, whereas P2- $Na_{0.56}[Mn_{0.86}\square_{0.14}]O_2$  just delivered the capacity retention of  $\sim 90.42\%$  at the same conditions. In terms of P2-NTMVO, moreover, the differential capacity vs voltage ( $dQ/dV$ ) profiles were stably retained for 100 cycles with no remarkable voltage decay [Fig. 2(f)], which is clearly different from the  $dQ/dV$  results of P2-NMVO that shows the dramatic voltage decay and the distinct deformation of its original profile for 100 cycles [Fig. 2(g)].

In particular, the outstanding electrochemical properties of P2-NTMVO were clearly distinguished through comparison with those of other cathode materials for NIBs. As shown in Fig. S23, it was confirmed that P2-NTMVO can deliver a larger specific capacity ( $\sim 224.92$  mAh  $g^{-1}$ ) and energy density capacity ( $\sim 589.3$  Wh  $kg^{-1}$ ) than other cathode materials.<sup>16,23,57–60</sup>

### C. Highly stabilized anionic redox reaction of P2-NTMVO

To understand the theoretical electrochemical properties of P2-NTMVO with stably occurring  $O^{2-}/O^-$  anionic redox reaction, we performed first-principles calculations. Various configurations of P2- $Na_x[Ti_{0.1}Mn_{0.76}\square_{0.14}]O_2$  were prepared using the CASM software.<sup>44</sup> Figure 3(a) presents the convex-hull plot on the formation energies of P2- $Na_x[Ti_{0.1}Mn_{0.76}\square_{0.14}]O_2$  with various Na contents ( $0 \leq x \leq 1$ ). The theoretical redox potentials of P2- $Na_x[Ti_{0.1}Mn_{0.76}\square_{0.14}]O_2$  were calculated using the following equation:

$$V = - \frac{E[Na_{x_2}[Ti_{0.1}Mn_{0.76}\square_{0.14}]O_2] - E[Na_{x_1}[Ti_{0.1}Mn_{0.76}\square_{0.14}]O_2] - (x_2 - x_1)E[Na]}{(x_2 - x_1)F} \quad (1)$$

where  $V$ ,  $E$ , and  $F$  indicate the average redox potentials, the most stable formation energy of each P2- $Na_x[Ti_{0.1}Mn_{0.76}\square_{0.14}]O_2$  composition, and the Faraday constant, respectively. These first-principles calculation results imply that more than 0.8 mol  $Na^+$  content can be reversibly and easily de/intercalated in the P2-NTMVO structure during charge/discharge. Figure 3(b) shows that the theoretical redox potentials of P2-NTMVO predicted by first-principles calculation were consistent with the experimentally measured charge/discharge curves at 13 mA  $g^{-1}$ . In particular, it was verified that values of the redox potentials between P2- $Na_x[Ti_{0.1}Mn_{0.76}\square_{0.14}]O_2$  compositions are dependent on the occurrence of the anionic-redox reaction of  $O^{2-}/O^-$ . Thus, the high-voltage regions by initial  $Na^+$  deintercalation from P2- $Na_{0.56}[Ti_{0.1}Mn_{0.76}\square_{0.14}]O_2$  were determined by the anionic redox reaction, and the relatively low-voltage regions by further  $Na^+$  intercalation are affected by the cationic redox reaction of  $Mn^{4+}/Mn^{3+}$ . The detailed anionic and cationic redox mechanisms of P2-NTMVO were investigated through comparison of the projected density of state (pDOS) of O 2p, Mn 3d, and Ti 3d orbitals among various P2- $Na_x[Ti_{0.1}Mn_{0.76}\square_{0.14}]O_2$  phases, where  $x = 1, 0.67, 0.44, 0.22$ , and 0 [Fig. 3(c)]. During the  $Na^+$  deintercalation from

$Na_1[Ti_{0.1}Mn_{0.76}\square_{0.14}]O_2$  and  $Na_{0.44}[Ti_{0.1}Mn_{0.76}\square_{0.14}]O_2$ , the electron densities of the Mn 3d orbital are mainly transformed to the hole density, implying the occurrence of the  $Mn^{3+}/Mn^{4+}$  cationic redox reaction in P2-NTMVO. Moreover, the O 2p orbital of  $Na_{0.44}[Ti_{0.1}Mn_{0.76}\square_{0.14}]O_2$  has more dominant electron densities near the Fermi level than the Mn 3d and Ti 3d orbitals, and the hole densities of the O 2p orbital gradually increased during further  $Na^+$  deintercalation to  $Na_0[Ti_{0.1}Mn_{0.76}\square_{0.14}]O_2$ . These results on the change of the O 2p orbital indicate the sequential and selective occurrence of  $O^{2-}/O^-$  redox reaction in P2-NTMVO. The anionic and cationic redox mechanism of P2-NTMVO was also confirmed through Bader charge analyses. Figure S24 shows changes of the net effective charges on Mn, Ti, and O ions in P2- $Na_x[Ti_{0.1}Mn_{0.76}\square_{0.14}]O_2$  depending on the Na content, which also indicates the occurrence of  $O^{2-}/O^-$  and  $Mn^{4+}/Mn^{3+}$  redox reactions in P2-NTMVO during charge/discharge. Interestingly, the  $Ti^{4+}$  cations did not participate in the overall redox reaction of P2-NTMVO during  $Na^+$  de/intercalation, which implies that the fixed valence state regarding charge/discharge enables the application of  $Ti^{4+}$  cations as the structural stabilizer for stable electrochemical behaviors of anionic-redox-based P2-NTMVO.



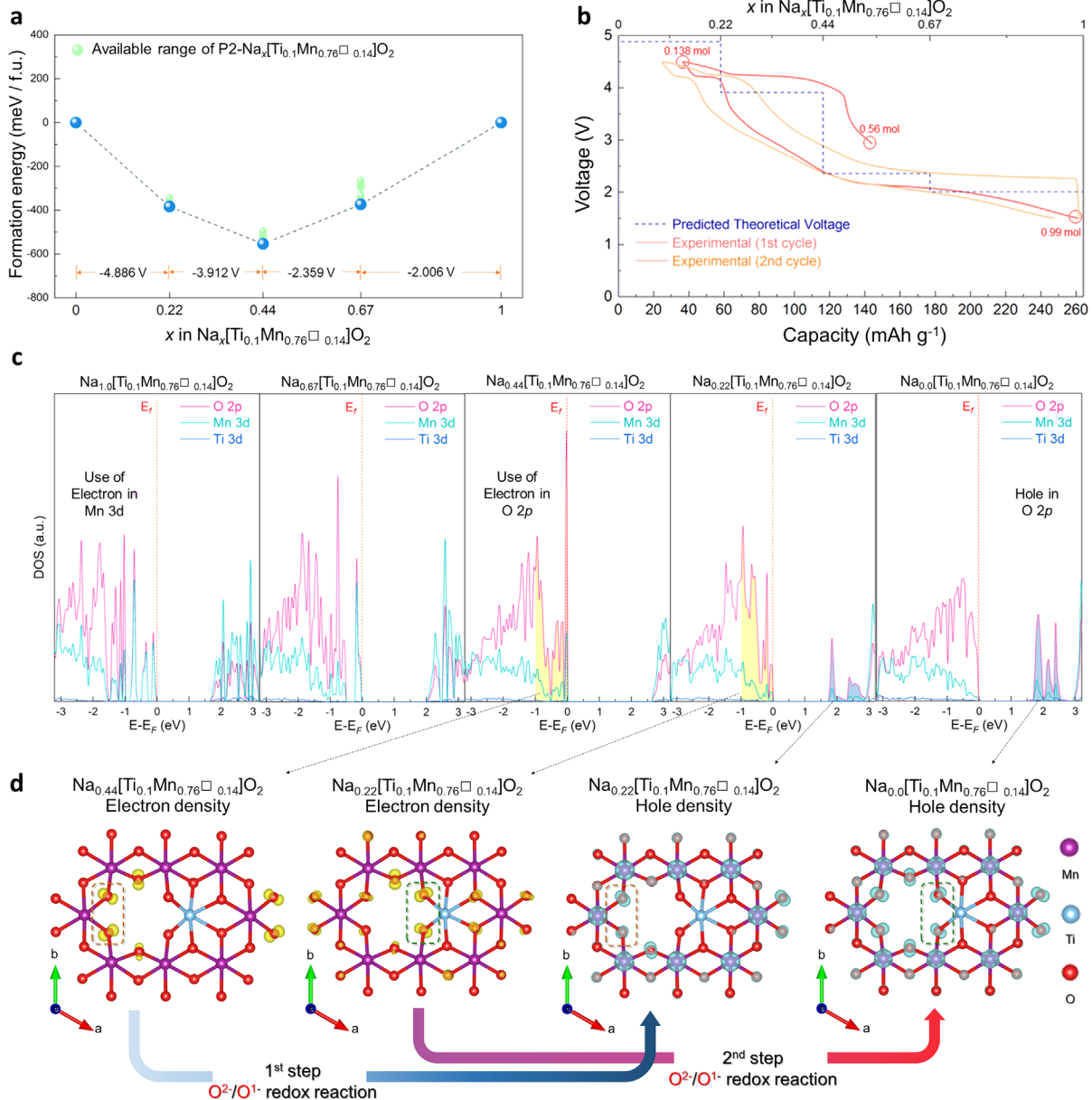


**FIG. 3.** (a) Convex-hull plot of  $\text{P2-Na}_x[\text{Ti}_{0.1}\text{Mn}_{0.76}\square_{0.14}]\text{O}_2$  configurations ( $0 \leq x \leq 1$ ). (b) Comparison of calculated redox potential of  $\text{P2-Na}_x[\text{Ti}_{0.1}\text{Mn}_{0.76}\square_{0.14}]\text{O}_2$  and its experimentally measured first and second cycle curves at  $13 \text{ mA g}^{-1}$ . (c) pDOS of O 2p, Mn 3d, and Ti 3d orbitals in  $\text{P2-Na}_x[\text{Ti}_{0.1}\text{Mn}_{0.76}\square_{0.14}]\text{O}_2$  ( $x = 1, 0.67, 0.44, 0.22, \text{ and } 0$ ). (d) Visualized pDOS of electron/hole density in  $\text{P2-Na}_x[\text{Ti}_{0.1}\text{Mn}_{0.76}\square_{0.14}]\text{O}_2$  ( $x = 1, 0.67, 0.44, 0.22, \text{ and } 0$ ).

The stabilizing effect of  $\text{Ti}^{4+}$  for improved electrochemical performances is also well matched with the several previous research papers.<sup>61–64</sup>

The visualization of the electron and hole densities of various  $\text{P2-Na}_x[\text{Ti}_{0.1}\text{Mn}_{0.76}\square_{0.14}]\text{O}_2$  clearly shows the effect of  $\text{Ti}^{4+}$  cations for the  $\text{O}^{2-}/\text{O}^{1-}$  redox mechanism in P2-NTMVO with vacancies in the (TM) layers [Fig. 3(d)]. In terms of  $\text{P2-Na}_{0.44}[\text{Ti}_{0.1}\text{Mn}_{0.76}\square_{0.14}]\text{O}_2$ , the electron densities at near the Fermi level are focused on the O 2p orbitals in the oxygen-anion neighboring vacancies in (TM) layers, indicating not Mn cations but O anions are oxidized during  $\text{Na}^+$  deintercalation from P2-

$\text{Na}_{0.44}[\text{Ti}_{0.1}\text{Mn}_{0.76}\square_{0.14}]\text{O}_2$ . Interestingly, it was verified that the electron densities in  $\text{P2-Na}_{0.44}[\text{Ti}_{0.1}\text{Mn}_{0.76}\square_{0.14}]\text{O}_2$  only exist at the oxygen anions binding manganese cations, and that there are no electron densities at the oxygen anions binding titanium cations. These results imply that oxygen anions binding manganese cations rather than titanium cations are preferentially oxidized. After  $\text{Na}^+$  deintercalation from  $\text{P2-Na}_{0.44}[\text{Ti}_{0.1}\text{Mn}_{0.76}\square_{0.14}]\text{O}_2$  to  $\text{P2-Na}_{0.22}[\text{Ti}_{0.1}\text{Mn}_{0.76}\square_{0.14}]\text{O}_2$ , the electron densities of oxygen anions binding manganese cations are transformed to the hole densities, and new electron densities are

observed at oxygen anions binding titanium cations. Figure S25 shows the pDOS of each oxygen anion neighboring manganese and titanium cations on  $P2\text{-Na}_x[\text{Ti}_{0.1}\text{Mn}_{0.76}\square_{0.14}]\text{O}_2$  ( $x = 0, 0.22, \text{ and } 0.44$ ), which also indicates that  $\text{O}^{2-}/\text{O}^-$  redox reaction sequentially and selectively occurred in  $P2\text{-Na}_x[\text{Ti}_{0.1}\text{Mn}_{0.76}\square_{0.14}]\text{O}_2$  through the existence of  $\text{Ti}^{4+}$  cations with fixed valence state regardless of charge/discharge. In particular, this sequential and selective anionic redox reaction by  $\text{Ti}^{4+}$  cations enables a small change of local environment after  $\text{Na}^+$  deintercalation. It was reported that the vacancy in [TM] layers can serve as a buffer for preventing large structural distortion during  $\text{Na}^+$  de/intercalation.<sup>65,66</sup> As presented in Fig. 4(a), the vacancy size of  $P2\text{-Na}_x[\text{Ti}_{0.1}\text{Mn}_{0.76}\square_{0.14}]\text{O}_2$  during  $\text{Na}^+$  deintercalation increased from 4.59 to 5.21  $\text{\AA}^2$ , indicating  $\sim 13.5\%$  change in the vacancy size, whereas  $P2\text{-Na}_x[\text{Mn}_{0.86}\square_{0.14}]\text{O}_2$  only exhibited a  $\sim 20.0\%$  change in the vacancy size [Fig. 4(b)]. The smaller change of local environments of  $P2\text{-Na}_x[\text{Ti}_{0.1}\text{Mn}_{0.76}\square_{0.14}]\text{O}_2$  than that of  $P2\text{-Na}_x[\text{Mn}_{0.86}\square_{0.14}]\text{O}_2$  implies that  $\text{Ti}^{4+}$  cations in  $P2\text{-NTMVO}$  can play a role as a structural stabilizer for stable and

sequential  $\text{O}^{2-}/\text{O}^-$  redox reaction and enhanced electrochemical behavior.

In addition, the overall cationic and anionic redox reactions in  $P2\text{-NTMVO}$  were confirmed through synchrotron-based *ex situ* XANES and soft x-ray absorption spectroscopy (sXAS) analyses. As observed in Fig. 5(a), the Mn K-edge of  $P2\text{-NTMVO}$  was negligibly shifted during the initial charge to 4.5 V, indicating the non-oxidation of  $\text{Mn}^{4+}$  cations in  $P2\text{-NTMVO}$  during  $\text{Na}^+$  deintercalation from  $P2\text{-NTMVO}$ . After discharging to 1.5 V, the Mn K-edge was shifted toward lower energy level, which is attributed to reduction from  $\text{Mn}^{4+}$  to  $\text{Mn}^{3+}$  by further  $\text{Na}^+$  intercalation. In terms of the Ti K-edge of  $P2\text{-NTMVO}$  [Fig. 5(b)], any considerable shift was not detected during charge/discharge, indicating that  $\text{Ti}^{4+}$  cations do not participate in the redox reactions of  $P2\text{-NTMVO}$  and play a role as the structural stabilizer for stable and reversible  $\text{O}^{2-}/\text{O}^-$  redox reaction. In a previous study, it was reported that inactive  $\text{Ti}^{4+}$  substitution helps to suppress oxygen release and increase structural stability because it has a

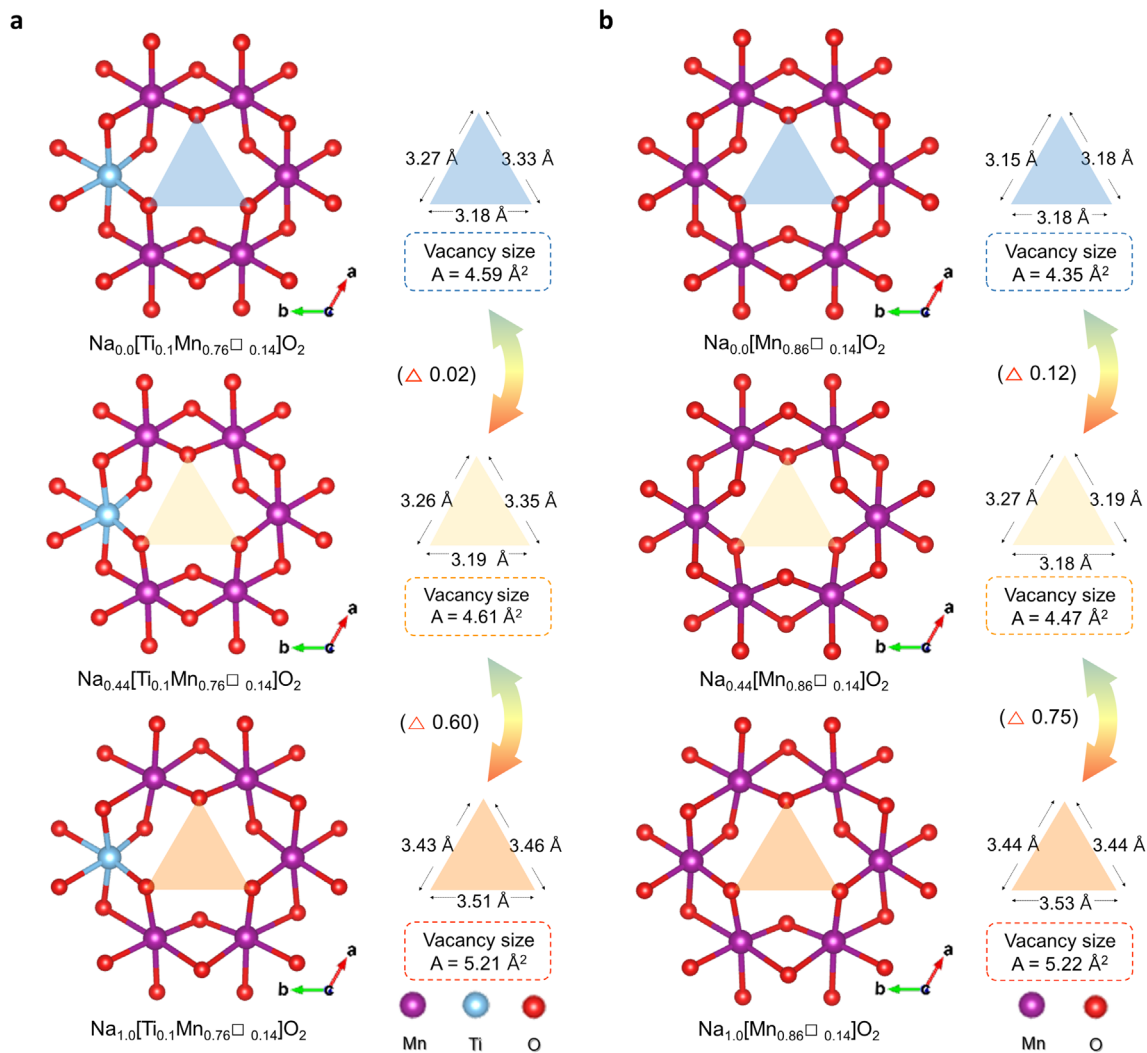
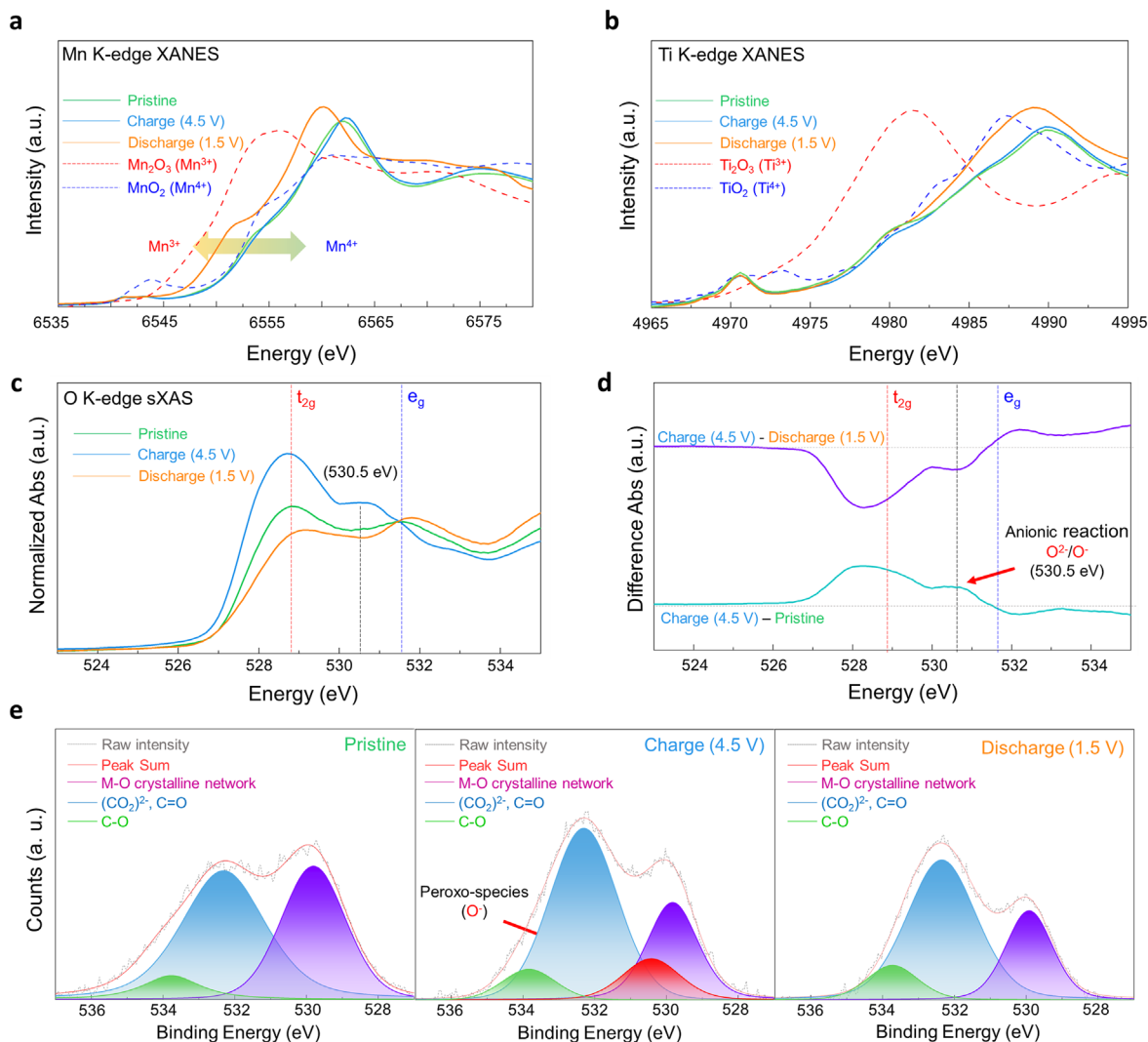


FIG. 4. Comparison of vacancy size of (a)  $P2\text{-Na}_x[\text{Ti}_{0.1}\text{Mn}_{0.76}\square_{0.14}]\text{O}_2$  and (b)  $P2\text{-Na}_x[\text{Mn}_{0.86}\square_{0.14}]\text{O}_2$  ( $x = 1, 0.44, \text{ and } 0$ ).



**FIG. 5.** *Ex situ* analyses of  $\text{P2-Na}_x[\text{Ti}_{0.1}\text{Mn}_{0.76}\square_{0.14}]\text{O}_2$  on (a) Mn K-edge XANES spectra and (b) Ti K-edge XANES spectra during charge/discharge. (c) O K-edge sXAS spectra of  $\text{Na}_{0.56}[\text{Ti}_{0.1}\text{Mn}_{0.76}\square_{0.14}]\text{O}_2$ . (d) Difference spectra on O K-edge of  $\text{P2-Na}_x[\text{Ti}_{0.1}\text{Mn}_{0.76}\square_{0.14}]\text{O}_2$ . (e) O 1s XPS spectra of the  $\text{P2-Na}_x[\text{Ti}_{0.1}\text{Mn}_{0.76}\square_{0.14}]\text{O}_2$ .

higher binding energy with oxygen ( $662 \text{ kJ mol}^{-1}$ ) than Mn–O ( $402 \text{ kJ mol}^{-1}$ ).<sup>67,68</sup> The extended x-ray absorption fine structure (EXAFS) analyses also reveal the elongation/shrinkage of Mn–O bond lengths, confirming the reversible cationic and anionic redox reaction of P2-NTMVO during charge/discharge (Fig. S26). Moreover, the occurrence of  $\text{O}^{2-}/\text{O}^-$  redox reaction was confirmed through sXAS analyses of the O K-edge spectra of P2-NTMVO [Fig. 5(c)]. During charging to 4.5 V, the intensity at 530.5 eV increased, resulting from the localized features of the oxidized oxygen anions.<sup>69</sup> The successive anionic redox reaction of  $\text{O}^{2-}/\text{O}^-$  was clearly confirmed through the plot showing the intensity difference between each O K-edge spectra [Fig. 5(d)]. Furthermore, *ex situ* x-ray photoelectron spectroscopy (XPS) analyses of the O 1s spectra of P2-NTMVO showed that the peroxo-like species ( $\sim 530.5 \text{ eV}$ ) reversibly appear/disappear during charge/discharge<sup>66,70,71</sup> at the 4.5 V charge state of P2-NTMVO,

further evidence of the occurrence of the reversible  $\text{O}^{2-}/\text{O}^-$  redox reaction in P2-NTMVO [Fig. 5(e)].

#### D. Effectively suppressed structural variation of P2-NTMVO during $\text{Na}^+$ de/intercalation

The outstanding electrochemical performance of P2-NTMVO resulted from the stably occurring anionic redox reaction through the existence of  $\text{Ti}^{4+}$  cations as a structural stabilizer, which is clearly backed up through effectively suppressed structural change of P2-NTMVO during  $\text{Na}^+$  de/intercalation compared with that of P2-NMVO. Figures 6(a) and 6(b) presents the *operando* XRD analyses of P2-NTMVO and P2-NMVO during charge/discharge. The full *operando* XRD patterns are presented in Fig. S27. Interestingly, unlike other P2-type Na-layered oxide cathodes, neither P2-NTMVO nor

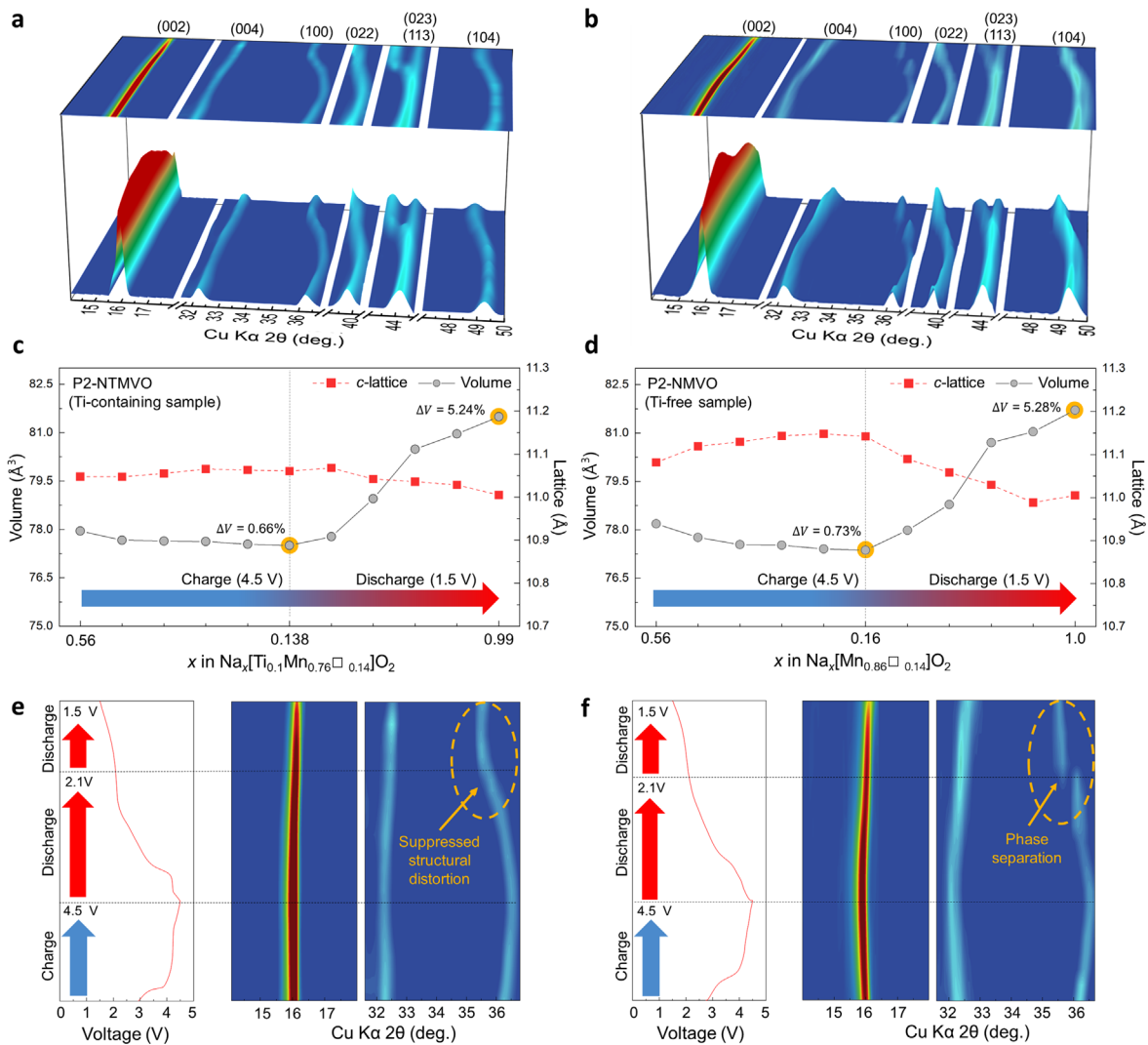


**FIG. 6.** (a and b) *Operando* XRD patterns of (a)  $\text{P2-Na}_{0.56}[\text{Ti}_{0.1}\text{Mn}_{0.76}\square_{0.14}]\text{O}_2$  and (b)  $\text{P2-Na}_{0.56}[\text{Mn}_{0.86}\square_{0.14}]\text{O}_2$ . (c) and (d) Change in  $c$ -lattice parameter and volume as a function of Na content in (c)  $\text{P2-Na}_{0.56}[\text{Ti}_{0.1}\text{Mn}_{0.76}\square_{0.14}]\text{O}_2$  and (d)  $\text{P2-Na}_{0.56}[\text{Mn}_{0.86}\square_{0.14}]\text{O}_2$ . (e) and (f) Magnified views of (e)  $\text{P2-Na}_{0.56}[\text{Ti}_{0.1}\text{Mn}_{0.76}\square_{0.14}]\text{O}_2$  and (f)  $\text{P2-Na}_{0.56}[\text{Mn}_{0.86}\square_{0.14}]\text{O}_2$  during charge/discharge.

P2-NMVO exhibited a large structural change such as P2-OP4 phase transition during charge,<sup>24–26</sup> implying that the presence of vacancies in (TM) layers can relax the severe structural deformation during  $\text{Na}^+$  deintercalation, enabling the structural retention of the P2-type layered oxide. However, it is not changed that the formation of oxidized oxygen anion during anionic redox reaction can result in local and overall structural change, despite the suppressed structural distortion. Through Rietveld refinement, we clearly demonstrated that 4.5 V-charged P2-NTMVO and P2-NMVO exhibit a P2-type layered structure without the phase transition (Fig. S28 and Table S8). Moreover, simple Ti-substitution in P2-type layered oxide cannot prevent the large structural change by the phase transition to OP4.<sup>72,73</sup> Thus, we expected existence of both  $\text{Ti}^{4+}$  cation and vacancy in the Mn site that can make a synergy to enable improved electrochemical properties by

the suppressed structural change and the stabilized anionic redox reaction of  $\text{O}^{2-}/\text{O}^-$ . As shown in Figs. 6(c) and 6(d), the variations of the  $c$ -lattice parameters and volume change of P2-NTMVO during charge were only  $\sim 0.12\%$  and  $\sim 0.66\%$ , respectively, which is much smaller than those of P2-NMVO. These results exhibited a large change of the lattice parameters ( $c$ -lattice:  $\sim 0.62\%$  and volume:  $\sim 0.73\%$ ). The decreased structural change by  $\text{Ti}^{4+}$  cations can lead to more stable  $\text{O}^{2-}/\text{O}^-$  redox reaction of P2-NTMVO than that of P2-NMVO. These results are also well matches with the DFT calculation results, showing that the vacancy in P2-NTMVO during  $\text{Na}^+$  deintercalation by anionic redox reaction was much less changed than that in P2-NMVO (Fig. 4). It implies that the structural distortion of P2-NTMVO by anionic redox reaction is more suppressed than that of P2-NMVO. Thus, we supposed that anionic redox reaction in



P2-NTMVO can be more stably and reversibly occurred than that in P2-NMVO.

Furthermore, the suppressed structural change of P2-NTMVO was clearly observed during the discharging process. Compared with P2-NMVO, P2-NTMVO exhibited a small variation of lattice parameters and volume (*c*-lattice:  $\sim 0.5\%$  and volume:  $\sim 5.24\%$ ) during discharge [Figs. 6(c) and 6(d)]. In particular, whereas P2-NMVO underwent a P2-P'2 phase transition with a clearly distinct two-phase reaction, the P2-P'2 phase transition of P2-NTMVO is based on a monotonous single-phase reaction [Figs. 6(e) and 6(f)], which implies the local environments of Mn-O bonds in P2-NTMVO are more smoothly changed during Na<sup>+</sup> intercalation than those in P2-NMVO. Thus, we confirmed that the presence of Ti<sup>4+</sup> cations as a structural stabilizer in the P2-NTMVO structure can effectively suppress the structural variation such as the change of lattice parameters and P2-OP4 and P2-P'2 phase transition, which enables a highly stable anionic redox reaction and excellent electrochemical behaviors of P2-NTMVO under the NIB system.

#### IV. CONCLUSION

In this work, we demonstrated that the synergy of vacancies and Ti<sup>4+</sup> cations in the (TM) layers can deliver effective stabilization of the anionic redox reaction and structure in P2-Na<sub>0.56</sub>[Ti<sub>0.1</sub>Mn<sub>0.76</sub>□<sub>0.14</sub>]O<sub>2</sub> (P2-NTMVO). During charge/discharge at a current density of 13 mA g<sup>-1</sup> (1C = 264.1 mA g<sup>-1</sup>), P2-NTMVO delivered a specific capacity and energy density of  $\sim 224.92$  mAh g<sup>-1</sup> and 589.3 Wh kg<sup>-1</sup>, respectively. These values are very large compared with those of previously reported cathode materials for NIBs. In particular, despite the anionic redox reaction being accompanied by large structural distortion, P2-NTMVO exhibited excellent cycle performance with a capacity retention of  $\sim 80.38\%$  for 200 cycles, implying a stabilized O<sup>2-</sup>/O<sup>-</sup> redox reaction in P2-NTMVO. Through first-principles calculation, it was verified that the combination of vacancies and Ti<sup>4+</sup> cations in the (TM) layers results in not only small distortion of the local structural environment but also sequential and selective anionic redox reaction of O<sup>2-</sup>/O<sup>-</sup>. In particular, the structural change of P2-NTMVO occurring during charge/discharge is clearly distinguished from that of other P2-type layered oxide cathode materials for NIBs. Moreover, the *operando* XRD data indicate well retained without P2-OP4 phase transition during charge/discharge, and that the P2-P'2 phase transition in P2-NTMVO occurred with a monotonous single-phase reaction. These findings support the outstanding electrochemical performance of P2-NTMVO with stabilized anionic and cationic redox reactions compared with that of other cathode materials for NIBs. Although the issue on low Na contents is one of the major problem of P2-NTMVO, the usage of sodiated hard carbon anode for NTMVO-based full cell showed the possibility of P2-NTMVO as the promising cathode for the realistic full cell of NIBs. We believe that our study provides an excellent strategy to enhance both anionic-redox-based electrochemical behaviors and structural stability in layered oxide cathode materials for high-energy and low-cost Na-ion batteries.

#### SUPPLEMENTARY MATERIAL

See the [supplementary material](#) associated with this article.

#### ACKNOWLEDGMENTS

This research was supported by the National Research Foundation of Korea (Nos. 2019M3D1A2104105 and 2021R1A2C1014280)

funded by the Ministry of Science and ICT of Korea (Nos. NRF-2019M2A2A6A05102365, NRF-2020M2D8A2070870, and NRF-2022M3H4A1A01010832). Also, this work was supported by the Korea Institute of Materials Science (KIMS) of the Republic of Korea (No. PNK7330) and the Supercomputing Center/Korea Institute of Science and Technology (No. KSC-2022-CRE-0030).

#### AUTHOR DECLARATIONS

##### Conflict of Interest

The authors have no conflicts to disclose.

##### Author Contributions

Sangyeop Lee and Jungmin Kang contributed equally to this work.

**Sangyeop Lee:** Conceptualization (equal); Data curation (equal); Formal analysis (equal); Investigation (equal); Resources (equal); Visualization (equal); Writing – original draft (equal); Writing – review & editing (equal). **Jungmin Kang:** Conceptualization (equal); Formal analysis (equal); Writing – review & editing (equal). **Min Kyung Cho:** Formal analysis (supporting). **Hyunyoung Park:** Data curation (supporting); Investigation (supporting). **Wonseok Ko:** Formal analysis (supporting). **Yongseok Lee:** Formal analysis (supporting). **Jinho Ahn:** Formal analysis (supporting). **Seokjin Lee:** Formal analysis (supporting). **Eunji Sim:** Formal analysis (supporting). **Kyuwook Ihm:** Formal analysis (supporting). **Jihyun Hong:** Writing – review & editing (supporting). **Hyungsub Kim:** Formal analysis (supporting); Investigation (supporting). **Jongsoo Kim:** Conceptualization (equal); Formal analysis (equal); Funding acquisition (equal); Investigation (equal); Supervision (equal); Writing – review & editing (equal).

#### DATA AVAILABILITY

The data that support the findings of this study are available from the corresponding author upon reasonable request.

#### REFERENCES

- <sup>1</sup>B. Dunn, H. Kamath, and J.-M. Tarascon, “Electrical energy storage for the grid: A battery of choices,” *Science* **334**, 928 (2011).
- <sup>2</sup>S. J. Davis, N. S. Lewis, M. Shaner, S. Aggarwal, D. Arent, I. L. Azevedo, S. M. Benson, T. Bradley, J. Brouwer, Y. M. Chiang, C. T. M. Clack, A. Cohen, S. Doig, J. Edmonds, P. Fennell, C. B. Field, B. Hannegan, B. M. Hodge, M. I. Hoffert, E. Ingersoll, P. Jaramillo, K. S. Lackner, K. J. Mach, M. Mastrandrea, J. Ogden, P. F. Peterson, D. L. Sanchez, D. Sperling, J. Stagner, J. E. Trancik, C. J. Yang, and K. Caldeira, “Net-zero emissions energy systems,” *Science* **360**, eaas9793 (2018).
- <sup>3</sup>J. B. Goodenough, “Electrochemical energy storage in a sustainable modern society,” *Energy Environ. Sci.* **7**, 14 (2014).
- <sup>4</sup>J. B. Goodenough, “How we made the Li-ion rechargeable battery,” *Nat. Electron.* **1**, 204 (2018).
- <sup>5</sup>D. Eum, B. Kim, S. J. Kim, H. Park, J. Wu, S.-P. Cho, G. Yoon, M. H. Lee, S.-K. Jung, W. Yang, W. M. Seong, K. Ku, O. Tamwattana, S. K. Park, I. Hwang, and K. Kang, “Voltage decay and redox asymmetry mitigation by reversible cation migration in lithium-rich layered oxide electrodes,” *Nat. Mater.* **19**, 419 (2020).
- <sup>6</sup>Z. Wang, L. Zhou, and X. W. Lou, “Metal oxide hollow nanostructures for lithium-ion batteries,” *Adv. Mater.* **24**, 1903 (2012).
- <sup>7</sup>V. Etacheri, R. Marom, R. Elazari, G. Salitra, and D. Aurbach, “Challenges in the development of advanced Li-ion batteries: A review,” *Energy Environ. Sci.* **4**, 3243 (2011).

- <sup>8</sup>T. Kim, W. Choi, H.-C. Shin, J.-Y. Choi, J. M. Kim, M.-S. Park, and W.-S. Yoon, "Applications of voltammetry in lithium ion battery research," *J. Electrochem. Sci. Technol.* **11**, 14 (2020).
- <sup>9</sup>S. Akhtar, W. Lee, M. Kim, M. S. Park, and W. S. Yoon, "Conduction mechanism of charge carriers in electrodes and design factors for the improvement of charge conduction in Li-ion batteries," *J. Electrochem. Sci. Technol.* **12**, 1 (2021).
- <sup>10</sup>S. W. Kim, D. H. Seo, X. Ma, G. Ceder, and K. Kang, "Electrode materials for rechargeable sodium-ion batteries: Potential alternatives to current lithium-ion batteries," *Adv. Energy Mater.* **2**, 710 (2012).
- <sup>11</sup>C. Wang, M. Sawicki, S. Emani, C. Liu, and L. L. Shaw, " $\text{Na}_3\text{MnCO}_3\text{PO}_4$ : A high capacity, multi-electron transfer redox cathode material for sodium ion batteries," *Electrochim. Acta* **161**, 322 (2015).
- <sup>12</sup>N. V. Kosova and A. A. Shindrov, "Mechanochemical synthesis of a new composite  $\text{Na}_3\text{FePO}_4\text{CO}_3/\text{C}$  cathode material for sodium-ion batteries," *Mater. Today Proc.* **12**, 3 (2019).
- <sup>13</sup>Y. Fang, X.-Y. Yu, and X. W. D. Lou, "Nanostructured electrode materials for advanced sodium-ion batteries," *Matter* **1**, 90 (2019).
- <sup>14</sup>S. Y. Hong, Y. Kim, Y. Park, A. Choi, N.-S. Choi, and K. T. Lee, "Charge carriers in rechargeable batteries: Na ions vs. Li ions," *Energy Environ. Sci.* **6**, 2067 (2013).
- <sup>15</sup>J. Hwang, J. Kim, T. Yu, and Y. Sun, "A new P2-type layered oxide cathode with extremely high energy density for sodium-ion batteries," *Adv. Energy Mater.* **9**, 1803346 (2019).
- <sup>16</sup>H. Kim, H. Kim, Z. Ding, M. H. Lee, K. Lim, G. Yoon, and K. Kang, "Recent progress in electrode materials for sodium-ion batteries," *Adv. Energy Mater.* **6**, 1600943 (2016).
- <sup>17</sup>U. Maitra, R. A. House, J. W. Somerville, N. Tapia-Ruiz, J. G. Lozano, N. Guerrini, R. Hao, K. Luo, L. Jin, M. A. Pérez-Osorio, F. Massel, D. M. Pickup, S. Ramos, X. Lu, D. E. McNally, A. V. Chadwick, F. Giustino, T. Schmitt, L. C. Duda, M. R. Roberts, and P. G. Bruce, "Oxygen redox chemistry without excess alkali-metal ions in  $\text{Na}_{2/3}[\text{Mg}_{0.28}\text{Mn}_{0.72}]\text{O}_2$ ," *Nat. Chem.* **10**, 288 (2018).
- <sup>18</sup>X. Bai, M. Sathiy, B. Mendoza-Sánchez, A. Iadecola, J. Vergnet, R. Dedyèvre, M. Saubanière, A. M. Abakumov, P. Rozier, and J.-M. Tarascon, "Anionic redox activity in a newly Zn-doped sodium layered oxide  $\text{P2-Na}_{2/3}\text{Mn}_{1-y}\text{Zn}_y\text{O}_2$  ( $0 < y < 0.23$ )," *Adv. Energy Mater.* **8**, 1802379 (2018).
- <sup>19</sup>L. Yang, L. Kuo, J. M. López del Amo, P. K. Nayak, K. A. Mazzio, S. Maletti, D. Mikhailova, L. Giebeler, P. Kaghazchi, T. Rojo, and P. Adelhelm, "Structural aspects of P2-type  $\text{Na}_{0.6}\text{Mn}_{0.6}\text{Ni}_{0.2}\text{Li}_{0.2}\text{O}_2$  (MNL) stabilization by lithium defects as a cathode material for sodium-ion batteries," *Adv. Funct. Mater.* **31**, 2102939 (2021).
- <sup>20</sup>R. Stoyanova, D. Carlier, M. Sendova-Vassileva, M. Yoncheva, E. Zhecheva, D. Nihitjanova, and C. Delmas, "Stabilization of over-stoichiometric  $\text{Mn}^{4+}$  in layered  $\text{Na}_{2/3}\text{MnO}_2$ ," *J. Solid State Chem.* **183**, 1372 (2010).
- <sup>21</sup>X. Liu, G. Zhong, Z. Xiao, B. Zheng, W. Zuo, K. Zhou, H. Liu, Z. Liang, Y. Xiang, Z. Chen, G. F. Ortiz, R. Fu, and Y. Yang, "Al and Fe-containing Mn-based layered cathode with controlled vacancies for high-rate sodium ion batteries," *Nano Energy* **76**, 104997 (2020).
- <sup>22</sup>S. Kumakura, Y. Tahara, K. Kubota, K. Chihara, and S. Komaba, "Sodium and manganese stoichiometry of P2-type  $\text{Na}_{2/3}\text{MnO}_2$ ," *Angew. Chem.-Int. Ed.* **55**, 12760 (2016).
- <sup>23</sup>N. Yabuuchi, M. Kajiyama, J. Iwatate, H. Nishikawa, S. Hitomi, R. Okuyama, R. Usui, Y. Yamada, and S. Komaba, "P2-type  $\text{Na}_x[\text{Fe}_{1/2}\text{Mn}_{1/2}]\text{O}_2$  made from earth-abundant elements for rechargeable Na batteries," *Nat. Mater.* **11**, 512 (2012).
- <sup>24</sup>H. Liu, X. Gao, J. Chen, J. Gao, S. Yin, S. Zhang, L. Yang, S. Fang, Y. Mei, X. Xiao, L. Chen, W. Deng, F. Li, G. Zou, H. Hou, and X. Ji, "Reversible OP4 phase in  $\text{P2-Na}_{2/3}\text{Ni}_{1/3}\text{Mn}_{2/3}\text{O}_2$  sodium ion cathode," *J. Power Sources* **508**, 230324 (2021).
- <sup>25</sup>N. Tapia-Ruiz, W. M. Dose, N. Sharma, H. Chen, J. Heath, J. W. Somerville, U. Maitra, M. S. Islam, and P. G. Bruce, "High voltage structural evolution and enhanced Na-ion diffusion in  $\text{P2-Na}_{2/3}\text{Ni}_{1/3-x}\text{Mg}_x\text{Mn}_{2/3}\text{O}_2$  ( $0 \leq x \leq 0.2$ ) cathodes from diffraction, electrochemical and *ab initio* studies," *Energy Environ. Sci.* **11**, 1470 (2018).
- <sup>26</sup>W. Zuo, J. Qiu, X. Liu, B. Zheng, Y. Zhao, J. Li, H. He, K. Zhou, Z. Xiao, Q. Li, G. F. Ortiz, and Y. Yang, "Highly-stable  $\text{P2-Na}_{0.67}\text{MnO}_2$  electrode enabled by lattice tailoring and surface engineering," *Energy Storage Mater.* **26**, 503 (2020).
- <sup>27</sup>B. Mortemard de Boisse, S. Nishimura, E. Watanabe, L. Lander, A. Tsuchimoto, J. Kikkawa, E. Kobayashi, D. Asakura, M. Okubo, and A. Yamada, "Highly reversible oxygen-redox chemistry at 4.1 V in  $\text{Na}_{4/7-x}[\square_{1/7}\text{Mn}_{6/7}]\text{O}_2$  ( $\square$ : Mn vacancy)," *Adv. Energy Mater.* **8**, 1800409 (2018).
- <sup>28</sup>N. Voronina, M. Y. Shin, H. J. Kim, N. Yaqoob, O. Guillon, S. H. Song, H. Kim, H. D. Lim, H. G. Jung, Y. Kim, H. K. Lee, K. S. Lee, K. Yazawa, K. Gotoh, P. Kaghazchi, and S. T. Myung, "Hysteresis-suppressed reversible oxygen-redox cathodes for sodium-ion batteries," *Adv. Energy Mater.* **12**, 2103939 (2022).
- <sup>29</sup>X. Bai, A. Iadecola, J. M. Tarascon, and P. Rozier, "Decoupling the effect of vacancies and electropositive cations on the anionic redox processes in Na based P2-type layered oxides," *Energy Storage Mater.* **31**, 146 (2020).
- <sup>30</sup>C. Ma, J. Alvarado, J. Xu, R. J. Clément, M. Kodur, W. Tong, C. P. Grey, and Y. S. Meng, "Exploring oxygen activity in the high energy P2-type  $\text{Na}_{0.78}\text{Ni}_{0.23}\text{Mn}_{0.69}\text{O}_2$  cathode material for Na-ion batteries," *J. Am. Chem. Soc.* **139**, 4835 (2017).
- <sup>31</sup>H. Ren, Y. Li, Q. Ni, Y. Bai, H. Zhao, and C. Wu, "Unraveling anionic redox for sodium layered oxide cathodes: Breakthroughs and perspectives," *Adv. Mater.* **34**, 2106171 (2022).
- <sup>32</sup>C. Zhao, Q. Wang, Y. Lu, Y.-S. Hu, B. Li, and L. Chen, "Review on anionic redox for high-capacity lithium- and sodium-ion batteries," *J. Phys. D* **50**, 183001 (2017).
- <sup>33</sup>J. Feng, S. Luo, Y. Dou, J. Cong, X. Liu, P. Li, S. Yan, Q. Wang, Y. Zhang, X. Lei, and J. Gao, "Facile design and synthesis of Co-free layered  $\text{O}_3$ -type  $\text{NaNi}_{0.2}\text{Mn}_{0.2}\text{Fe}_{0.6}\text{O}_2$  as promising cathode material for sodium-ion batteries," *J. Electroanal. Chem.* **914**, 116301 (2022).
- <sup>34</sup>J. U. Choi, J. H. Jo, Y. J. Park, K. Lee, and S. Myung, "Mn-rich P'2- $\text{Na}_{0.67}[\text{Ni}_{0.1}\text{Fe}_{0.1}\text{Mn}_{0.8}]\text{O}_2$  as high-energy-density and long-life cathode material for sodium-ion batteries," *Adv. Energy Mater.* **10**, 2001346 (2020).
- <sup>35</sup>B. M. De Boisse, D. Carlier, M. Guignard, L. Bourgeois, and C. Delmas, " $\text{P}_2\text{-Na}_x\text{Mn}_{1/2}\text{Fe}_{1/2}\text{O}_2$  phase used as positive electrode in Na batteries: Structural changes induced by the electrochemical (de)intercalation process," *Inorg. Chem.* **53**, 11197 (2014).
- <sup>36</sup>X. Chen, X. Zhou, M. Hu, J. Liang, D. Wu, J. Wei, and Z. Zhou, "Stable layered  $\text{P3/P2 Na}_{0.66}\text{Co}_{0.5}\text{Mn}_{0.5}\text{O}_2$  cathode materials for sodium-ion batteries," *J. Mater. Chem. A* **3**, 20708 (2015).
- <sup>37</sup>J. Rodríguez-Carvajal, "Recent advances in magnetic structure determination by neutron powder diffraction," *Physica B* **192**, 55 (1993).
- <sup>38</sup>K. Luo, M. R. Roberts, N. Guerrini, N. Tapia-Ruiz, R. Hao, F. Massel, D. M. Pickup, S. Ramos, Y.-S. Liu, J. Guo, A. V. Chadwick, L. C. Duda, and P. G. Bruce, "Anion redox chemistry in the cobalt free 3d transition metal oxide intercalation electrode  $\text{Li}[\text{Li}_{0.2}\text{Ni}_{0.2}\text{Mn}_{0.6}]\text{O}_2$ ," *J. Am. Chem. Soc.* **138**, 11211 (2016).
- <sup>39</sup>F. P. Leitzke, R. O. C. Fonseca, J. Göttlicher, R. Steininger, S. Jahn, C. Prescher, and M. Lagos, "Ti K-edge XANES study on the coordination number and oxidation state of titanium in pyroxene, olivine, armalcolite, ilmenite, and silicate glass during mare basalt petrogenesis," *Contrib. Mineral. Petrol.* **173**, 103 (2018).
- <sup>40</sup>G. Kresse and J. Furthmüller, "Efficiency of *ab-initio* total energy calculations for metals and semiconductors using a plane-wave basis set," *Comput. Mater. Sci.* **6**, 15 (1996).
- <sup>41</sup>P. E. Blöchl, "Projector augmented-wave method," *Phys. Rev. B* **50**, 17953 (1994).
- <sup>42</sup>A. Jain, G. Hautier, S. P. Ong, C. J. Moore, C. C. Fischer, K. A. Persson, and G. Ceder, "Formation enthalpies by mixing GGA and GGA + U calculations," *Phys. Rev. B* **84**, 045115 (2011).
- <sup>43</sup>Y. Wang, J. Liu, B. Lee, R. Qiao, Z. Yang, S. Xu, X. Yu, L. Gu, Y. S. Hu, W. Yang, K. Kang, H. Li, X. Q. Yang, L. Chen, and X. Huang, "Ti-substituted tunnel-type  $\text{Na}_{0.44}\text{MnO}_2$  oxide as a negative electrode for aqueous sodium-ion batteries," *Nat. Commun.* **6**, 6401 (2015).
- <sup>44</sup>A. Van der Ven, J. C. Thomas, Q. Xu, and J. Bhattacharya, "Linking the electronic structure of solids to their thermodynamic and kinetic properties," *Math. Comput. Simul.* **80**, 1393 (2010).
- <sup>45</sup>C. Li, C. Zhao, B. Hu, W. Tong, M. Shen, and B. Hu, "Unraveling the critical role of Ti substitution in  $\text{P}_2\text{-Na}_x\text{Li}_y\text{Mn}_{1-y}\text{O}_2$  cathodes for highly reversible oxygen redox chemistry," *Chem. Mater.* **32**, 1054 (2020).

- <sup>46</sup>L. Yang, Z. Liu, X. Shen, S. Li, Z. Hu, Q. Kong, J. Ma, J. Li, H. J. Lin, C. Te Chen, J. M. Chen, S. C. Haw, X. Wang, R. Yu, Z. Wang, and L. Chen, "Effect of vacancy-tailored Mn<sup>3+</sup> spinning on enhancing structural stability," *Energy Storage Mater.* **44**, 231 (2022).
- <sup>47</sup>L. Yang, Z. Liu, S. Liu, M. Han, Q. Zhang, L. Gu, Q. Li, Z. Hu, X. Wang, H.-J. Lin, C.-T. Chen, J.-M. Chen, S.-C. Haw, Z. Wang, and L. Chen, "Superiority of native vacancies in activating anionic redox in P2-type Na<sub>2/3</sub>[Mn<sub>7/9</sub>Mg<sub>1/9</sub>□<sub>1/9</sub>]O<sub>2</sub>," *Nano Energy* **78**, 105172 (2020).
- <sup>48</sup>N. Jain and A. Roy, "Phase & morphology engineered surface reducibility of MnO<sub>2</sub> nano-heterostructures: Implications on catalytic activity towards CO oxidation," *Mater. Res. Bull.* **121**, 110615 (2020).
- <sup>49</sup>X. Gao, L. He, J. Xu, X. Chen, and H. He, "Facile synthesis of P25@Pd core-shell catalyst with ultrathin Pd shell and improved catalytic performance in heterogeneous enantioselective hydrogenation of acetophenone," *Catalysts* **9**, 513 (2019).
- <sup>50</sup>A. W. Hutchison, "The manganous ion-manganese dioxide electrode," *J. Am. Chem. Soc.* **69**, 3051 (1947).
- <sup>51</sup>J. J. Lingane and R. Karplus, "New method for determination of manganese," *Ind. Eng. Chem. Anal. Ed.* **18**, 191 (1946).
- <sup>52</sup>Y. Zhu, X. Liang, H. Zhao, H. Yin, M. Liu, F. Liu, and X. Feng, "Rapid determination of the Mn average oxidation state of Mn oxides with a novel two-step colorimetric method," *Anal. Methods* **9**, 103 (2017).
- <sup>53</sup>J. H. Jo, J. U. Choi, Y. J. Park, J. K. Ko, H. Yashiro, and S. T. Myung, "A new pre-sodiation additive for sodium-ion batteries," *Energy Storage Mater.* **32**, 281 (2020).
- <sup>54</sup>W. M. Dose and C. S. Johnson, "Cathode pre-lithiation/sodiation for next-generation batteries," *Curr. Opin. Electrochem.* **31**, 100827 (2022).
- <sup>55</sup>D. Eum, B. Kim, J.-H. Song, H. Park, H.-Y. Jang, S. J. Kim, S.-P. Cho, M. H. Lee, J. H. Heo, J. Park, Y. Ko, S. K. Park, J. Kim, K. Oh, D.-H. Kim, S. J. Kang, and K. Kang, "Coupling structural evolution and oxygen-redox electrochemistry in layered transition metal oxides," *Nat. Mater.* **21**, 664 (2022).
- <sup>56</sup>X. Rong, J. Liu, E. Hu, Y. Liu, Y. Wang, J. Wu, X. Yu, K. Page, Y.-S. Hu, W. Yang, H. Li, X.-Q. Yang, L. Chen, and X. Huang, "Structure-induced reversible anionic redox activity in Na layered oxide cathode," *Joule* **2**, 125 (2018).
- <sup>57</sup>M. H. Han, E. Gonzalo, N. Sharma, J. M. López Del Amo, M. Armand, M. Avdeev, J. J. Saiz Garitaonandia, and T. Rojo, "High-performance P2-phase Na<sub>2/3</sub>Mn<sub>0.8</sub>Fe<sub>0.1</sub>Ti<sub>0.1</sub>O<sub>2</sub> cathode material for ambient-temperature sodium-ion batteries," *Chem. Mater.* **28**, 106 (2016).
- <sup>58</sup>X. Rong, E. Hu, Y. Lu, F. Meng, C. Zhao, X. Wang, Q. Zhang, X. Yu, L. Gu, Y. S. Hu, H. Li, X. Huang, X. Q. Yang, C. Delmas, and L. Chen, "Anionic redox reaction-induced high-capacity and low-strain cathode with suppressed phase transition," *Joule* **3**, 503 (2019).
- <sup>59</sup>J. Wang, Y. Wang, D. Seo, T. Shi, S. Chen, Y. Tian, H. Kim, and G. Ceder, "A high-energy NASICON-type cathode material for Na-ion batteries," *Adv. Energy Mater.* **10**, 1903968 (2020).
- <sup>60</sup>Y. Lyu, Y. Liu, Z. E. Yu, N. Su, Y. Liu, W. Li, Q. Li, B. Guo, and B. Liu, "Recent advances in high energy-density cathode materials for sodium-ion batteries," *Sustainable Mater. Technol.* **21**, e00098 (2019).
- <sup>61</sup>Y. Wang, W. Zhu, A. Guerfi, C. Kim, and K. Zaghbi, "Roles of Ti in electrode materials for sodium-ion batteries," *Front. Energy Res.* **7**, 28 (2019).
- <sup>62</sup>Q. Zhao, F. K. Butt, Z. Guo, L. Wang, Y. Zhu, X. Xu, X. Ma, and C. Cao, "High-voltage P2-type manganese oxide cathode induced by titanium gradient modification for sodium ion batteries," *Chem. Eng. J.* **403**, 126308 (2021).
- <sup>63</sup>X. Cao, X. Li, Y. Qiao, M. Jia, F. Qiu, Y. He, P. He, and H. Zhou, "Restraining oxygen loss and suppressing structural distortion in a newly Ti-substituted layered oxide P2-Na<sub>0.66</sub>Li<sub>0.22</sub>Ti<sub>0.15</sub>Mn<sub>0.63</sub>O<sub>2</sub>," *ACS Energy Lett.* **4**, 2409 (2019).
- <sup>64</sup>C. Zhao, Z. Yao, J. Wang, Y. Lu, X. Bai, A. Aspuru-Guzik, L. Chen, and Y. S. Hu, "Ti substitution facilitating oxygen oxidation in Na<sub>2/3</sub>Mg<sub>1/3</sub>Ti<sub>1/6</sub>Mn<sub>1/2</sub>O<sub>2</sub> cathode," *Chem* **5**, 2913 (2019).
- <sup>65</sup>B. Song, M. Tang, E. Hu, O. J. Borkiewicz, K. M. Wiaderek, Y. Zhang, N. D. Phillip, X. Liu, Z. Shadik, C. Li, L. Song, Y.-Y. Hu, M. Chi, G. M. Veith, X.-Q. Yang, J. Liu, J. Nanda, K. Page, and A. Huq, "Understanding the low-voltage hysteresis of anionic redox in Na<sub>2</sub>Mn<sub>3</sub>O<sub>7</sub>," *Chem. Mater.* **31**, 3756 (2019).
- <sup>66</sup>Y. Li, X. Wang, Y. Gao, Q. Zhang, G. Tan, Q. Kong, S. Bak, G. Lu, X.-Q. Yang, L. Gu, J. Lu, K. Amine, Z. Wang, and L. Chen, "Native vacancy enhanced oxygen redox reversibility and structural robustness," *Adv. Energy Mater.* **9**, 1803087 (2019).
- <sup>67</sup>Z. Yu, S.-L. Shang, M. L. Gordin, A. Mousharraf, Z.-K. Liu, and D. Wang, "Ti-substituted Li [Li<sub>0.26</sub>Mn<sub>0.6-x</sub>Ti<sub>x</sub>Ni<sub>0.07</sub>Co<sub>0.07</sub>]O<sub>2</sub> layered cathode material with improved structural stability and suppressed voltage fading," *J. Mater. Chem. A* **3**, 17376 (2015).
- <sup>68</sup>X.-H. Ma, L.-L. Li, L. Cheng, F. Qiao, Y.-Y. Ye, N. Li, M.-L. Sha, Z.-F. Zi, and J.-M. Dai, "P2-type Na<sub>0.8</sub>(Li<sub>0.33</sub>Mn<sub>0.67-x</sub>Ti<sub>x</sub>)O<sub>2</sub> doped by Ti as cathode materials for high performance sodium-ion batteries," *J. Alloys Compd.* **815**, 152402 (2020).
- <sup>69</sup>J. Ahn, J. Kang, M. kyung Cho, H. Park, W. Ko, Y. Lee, H. S. Kim, Y. H. Jung, T. Y. Jeon, H. Kim, W. H. Ryu, J. Hong, and J. Kim, "Selective anionic redox and suppressed structural disordering enabling high-energy and long-life Li-rich layered-oxide cathode," *Adv. Energy Mater.* **11**, 2102311 (2021).
- <sup>70</sup>E. McCalla, A. M. Abakumov, M. Saubanère, D. Foix, E. J. Berg, G. Rousse, M.-L. Doublet, D. Gonbeau, P. Novák, G. Van Tendeloo, R. Dominko, and J.-M. Tarascon, "Visualization of O-O peroxo-like dimers in high-capacity layered oxides for Li-ion batteries," *Science* **350**, 1516 (2015).
- <sup>71</sup>M. Islam, M. Akbar, D. Han, B. Ali, Y. Jeong Choi, J. Lee, G. Choi, J.-H. Park, J.-Y. Kim, H.-G. Jung, K. Yoon Chung, D. Kim, Y.-M. Kang, and K.-W. Nam, "Unraveling vacancy-induced oxygen redox reaction and structural stability in Na-based layered oxides," *Chem. Eng. J.* **431**, 133962 (2022).
- <sup>72</sup>D. Pahari and S. Puravankara, "On controlling the P2-O2 phase transition by optimal Ti-substitution on Ni- site in P2-type Na<sub>0.67</sub>Ni<sub>0.33</sub>Mn<sub>0.67</sub>O<sub>2</sub> (NNMO) cathode for Na-ion batteries," *J. Power Sources* **455**, 227957 (2020).
- <sup>73</sup>J. Zhai, H. Ji, W. Ji, R. Wang, Z. Huang, T. Yang, C. Wang, T. Zhang, Z. Chen, W. Zhao, A. Tayal, L. Jin, J. Wang, and Y. Xiao, "Suppressing the irreversible phase transition in sodium layered cathode via integrating P2 and O3-type structures," *Mater. Today Energy* **29**, 101106 (2022).